Non-peer reviewed preprint submitted to EarthArXiv

Natural sampling and aliasing of marine geochemical signals

Andrew Curtis[1*] (andrew.curtis@ed.ac.uk)

Hugo Bloem[1] (hugo.bloem@ed.ac.uk)

Rachel Wood[1] (rachel.wood@ed.ac.uk)

Fred Bowyer[1] (fred.bowyer@ed.ac.uk)

Graham A. Shields[2] (g.shields@ucl.ac.uk)

Ying Zhou[2] (y-zhou@ucl.ac.uk)

Mariana Yilales[1] (m.a.yilales-agelvis@sms.ed.ac.uk)

Daniel Tetzlaff[3] (dan@westchasesoftware.com)

[1]School of GeoSciences, University of Edinburgh, James Hutton Road, Edinburgh, EH9 3FE, UK

[2]Department of Earth Sciences, University College London, Gower Street, London, WC1E 6BT, UK

[3]Westchase Software, Texas 77063, USA

*Corresponding Author: Andrew.Curtis@ed.ac.uk

ABSTRACT

It is well known that the sedimentary rock record is both incomplete and biased. Correlation between geographically distinct records is problematic in the absence of absolute age constraints, which can profoundly affect interpretations of geological and geochemical data. We use a computational process model to create canonical examples of carbonate-siliciclastic stratigraphic cross-sections from oscillatory overall-rising and -falling sea level, in which we can quantify how spatial and temporal geochemical records are biased by the inherent processes of marine sedimentation and preservation. Sedimentary hiatuses are shown to span ~50 to 95% of geological time, and even in these simple cases, infinitely dense sedimentology and geochemical data collected along spatial transects crossing the geological strata are shown to confound expert interpretations of paleo-environmental signals. Observations of secular variation of inferred paleo-environmental changes are shown to be irreversibly disguised as lower frequency signals by an aliasing effect, caused by cyclical and multiscale relative sea-level changes. Nyquist's theorem correctly predicts their biased signatures, proving that aliasing is caused by natural geological processes. Both effects are compounded by finite spatial sampling intervals adopted in practice, illustrated using real data case studies. These combined effects imply (a) that deeper marine records are significantly more likely to provide unaliased environmental signatures, and (b) that careful sedimentological field observations still allow such records to be correctly correlated in age given aliased shallow marine intervals.

1. Introduction

Accurate geochronological constraints are fundamental to our understanding of the evolution of the Earth, as they determine both how a geological succession might be correlated regionally and globally, and the temporal and spatial dynamics of any secular change (e.g., compare Kerans et al., 2014 with Wu et al., 2020). We know, however, that the sedimentary rock record is incomplete, and numerical simulations show it to be biased by facies variations, hiatuses including unconformities, and sampling (see Holland, 2023; Holland and Patzkowsky, 1999, 2015; Grocke, 2020). Sample ages between dateable strata must be estimated by interpolation which is usually piecewise-linear. Depositional hiatuses are sometimes inferred in order to improve the correlation between data from disparate localities (e.g., Hay et al., 2019; Eichenseer et al., 2023), which are usually taken along sub-vertical transects. This methodology often leads to poorly constrained spatio-temporal sampling relationships because hiatus ages and durations are unknown, e.g., if a hiatus occurs between each pair of consecutive samples then sample ages are almost arbitrary, constrained only by the law of superposition. Improving the accuracy of the temporal interpretation of spatially distributed data reduces the risk that true correlations are missed, and that spurious correlations are used to inform paleo-environmental change.

Sequence stratigraphic analysis suggests that the spatial position at which any sedimentary facies is deposited migrates laterally during sea level fluctuations in a predictable way (Fig. 1A). The result is that a profile that samples depositional age uniformly in shallow marine sediments must usually migrate laterally as well as vertically (Catuneanu et al., 2009). In the resulting sedimentary sequence, the age of deposition therefore varies nonlinearly along any spatially-linear transect that contains near-shore facies, and sub-vertical transects typically cross unconformities. The age of deposition changes abruptly

across an unconformity, and in the absence of directly dateable lithologies deposited before and after the hiatus, the length of time missing from the record (Fig. 1B) cannot easily be constrained without careful analysis of surrounding sediments.

Knowledge of the water depth in which a sediment is deposited is critical to interpretation of geochemical signatures, as the biological carbon pump leads to vertical depth gradients in isotopic ratios (e.g. carbon, barium, cadmium, etc.), nutrient concentrations and redox conditions, and in the modern these are highly variable regionally (Morel et al., 2014). Where significant, such gradients produce chemical disparities between contemporaneous sites that are due only to different relative depths of deposition. Temporal changes in geochemical signatures and depth gradients may then be confounded with relative sea level changes in geochemical proxy data observed along individual vertical transects. Increasing discrepancy can occur within the transgressive systems tract of the deep basin, in far upslope settings, and near the shelf break of the late highstand to early lowstand. For example, numerical simulations show that time is spatially condensed near predictable sedimentary surfaces such as maximum flooding surfaces (MFS) and sequence boundaries, driven by decreasing sedimentation, erosion and changes in water depth (Holland and Patzkowsky, 2015).

Figure 1: Mixed carbonate-siliciclastic sequence and $\delta^{13}C$ data on a rimmed shelf. A: Schematic, with facies distributions and major surfaces (sequence boundaries/correlative conformities (CC); transgressive surfaces; maximum flooding surfaces; parasequence boundaries) through a full and succeeding partial sequence. The shoreline trajectory traces the timeline of sediment at a fixed water depth through time. B: A Wheeler diagram of (A) showing the actual distribution of facies in space (landward to seaward) and through time. Horizontal lines show non-deposition. Modified from (Sonnenfeld, 1993). VE is vertical exaggeration. C: $\delta^{13}C$ data from a vertical succession through a mixed carbonate-siliciclastic ramp succession at Brak, Ediacaran Nama Group (Omkyk Member), Namibia, showing the distribution of lithologies and the position of parasequence boundaries. Modified from (Wood et al., 2015).

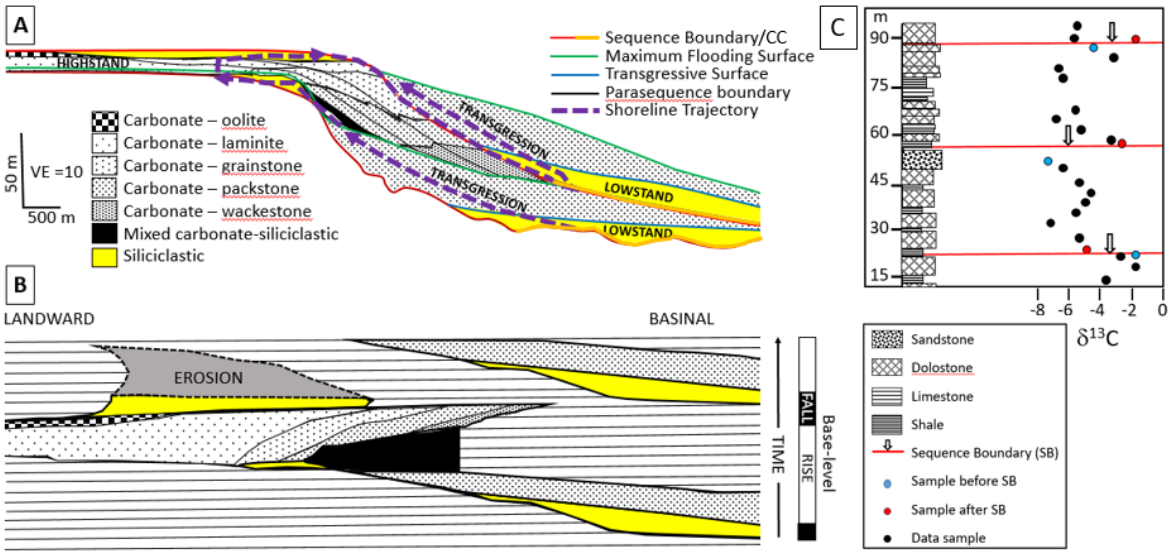

Sampling practice can also further limit our understanding of any given record. Often only a narrow range of lithologies such as carbonates or cemented mudstones is sampled (particularly in outcrop), ignoring other lithologies such as shale which may be poorly exposed, friable, and yet may represent the largest proportion of time in any given succession (6). In some cases, stratigraphically-connected samples of different lithologies are studied separately, so that a comprehensive understanding based on geochemical data is lacking. Finally, carbonate rocks have highly variable proportions of depositional versus diagenetic, or neritic versus pelagic components (e.g., Bodin et al., 2023), and these proportions can vary between different geological settings and different intervals of geological history, thus complicating their utility as consistent environmental indicators.

These issues are illustrated in carbon isotope ($\delta^{13}C$) data from a ca. 80 m vertical transect through a terminal Ediacaran mixed carbonate-clastic ramp succession (Wood et al., 2015), in which we note several phenomena (Fig. 1C). First, there is a considerable offset, in this case up to ca. 3 to 4.5 ‰, in sample $\delta^{13}C$ values found closely below and above the three traversed parasequence boundaries. These are present as abrupt shifts to both more negative and more positive values, despite an expectation (Figs. 1A,B) that the sign of the change would be consistent across each cycle boundary. Second, there is considerable variability in $\delta^{13}C$ values within any one sequence, up to ca. 4.5 ‰, but successive values generally present as either smooth negative or positive trends. The variety of lithologies present within a sequence include shale, limestone, dolostone and sandstone, suggesting that these follow relative, cyclical sea level trends during the deposition of a sequence, potentially explaining the smoothness of $\delta^{13}C$ trends. Finally, abrupt offsets are present, e.g., at ca. 80-85 m, which cannot readily be explained by the stratigraphic dynamics shown in Figure 1. In sum, these observations indicate that there is far greater complexity in the interpretation of such vertical $\delta^{13}C$ transects than is normally appreciated, and a more sophisticated sequence model than that idealised in Fig. 1A is required.

While many of these sampling issues have long been recognized and idealized sampling strategies for stratigraphic sections with time-constrained intervals proposed (e.g. see review 6), they have rarely been quantified (Myrow and Grotzinger, 2000). Here we use a geological process model to generate simple, canonical examples of carbonate-siliciclastic stratigraphic cross-sections from oscillatory overall-rising and -falling sea level, in which we can quantify the temporal distribution of spatially distributed data and the duration of hiatuses. We use these examples to highlight resultant issues of regional correlation, and show how intrinsic processes that control shallow marine sedimentation can create datasets that are in fact irreversibly disguised by aliasing – a phenomenon in which rapid variations present at far

lower spatiotemporal frequencies. Field data confirm these results, and lead us to conclude that contemporaneous transects above and below wave-base may often present ostensibly unrelated paleo-environmental signatures.

2. Methods

We use a geological process model (GPM) called *SedSimple* (Tetzlaff, 2023) to generate exemplar mixed carbonate-siliciclastic shelf margin sedimentary sequences. A GPM is a numerical simulation of dynamic processes acting over geological timescales (Burgess and Wright, 2003; Hill et al., 2009; Tetzlaff and Harbaugh, 1989). The range of processes included depends on the environment to be modelled, but for sedimentary environments typically includes most of sedimentary deposition, carbonate growth, erosion, transportation, re-deposition, and tectonic processes (Warrlich et al., 2008). Given a base topography, relative sea level as a function of time, and rate of carbonate production as a function of water depth, the GPM simulates sedimentary siliciclastic deposition and carbonate production, plus erosion and redistribution of both sediment types, resulting in a three-dimensional sedimentary volume. *SedSimple* is designed for rapid execution while simulating all of the above processes.

We simulate 5 Myr during which we form five parasequences due to relative sea level oscillations of 1 Myr duration, and compare a scenario of overall (time-averaged) rising sea-level with one of overall falling sea-level across an initial topography of a platform to basin profile, with carbonate growth rate a function of water depth (Figure S1). We refer to relative sea level simply as sea level – the effects of subsidence are implicit. Our simulation includes deposition, carbonate growth, erosion, sedimentary diffusion and re-deposition. We model three discrete facies which become mixed during diffusion: two siliciclastic facies of different grain sizes and one carbonate facies.

The simulated model contains the proportion of each facies at every 3D location and time step. It provides information on when and where each facies was deposited, which in combination with sea level variations allows water depth at time of deposition to be inferred throughout the model. We further model the $\delta^{13}C$ values recorded in sediment as linearly decreasing with depositional water depth, values also available throughout the model.

We finely sample six vertical transects spaced regularly between basinward and landward positions, simulating ultra-dense sub-vertical geochemical sampling on each transect. These logs are then interpolated to time, assuming the uncommonly fortunate scenario that a dated horizon such as an ash bed is available at the bottom (0 Myr) and top (5 Myr) of the succession. Data on each log are interpolated linearly between these ages to create temporal logs, as is common practice. The resulting logs represent idealised representations of geochemical data sets, from multiple, well-distributed transects with essentially continuous spatial sampling. This represents far denser sampling than is currently undertaken in practice.

Many examples are known of major $\delta^{13}C$ gradients with water depth, such as the modern Baltic Sea (e.g., Morel et al., 2014), and the Mesoproterozoic Wumishan Formation (e.g., Wang et al., 2022) and Ediacaran successions (e.g., Lu et al.., 2013) of south China. Here we use a Cryogenian case study which demonstrates differences in $\delta^{13}C$ of between 8 and 11‰ from back-reef to basin as an example gradient of stratification of $\delta^{13}C$ with water depth (Giddings and Wallace, 2009). While this might appear an extreme example, scaling the gradient by any factor (e.g., 0.5 for a desired gradient of 5‰) simply scales our simulated geochemical values by the same factor.

To illustrate the issues faced by stratigraphers using lithostratigraphy and $\delta^{13}C$ data for correlation across a shelf, we asked a stratigrapher experienced in regional and global correlation to correlate the two modelled sets of vertical transects of lithological transitions

and $\delta^{13}C$ data. They were told only that the logs were from transects spaced 5 km apart arranged basinward to landward across a shelf, and that they were modelled computationally from a GPM, thus explaining the apparently continuous rather than discrete vertical sampling of the data. Their justification for their interpretation is given in the Supplementary Materials.

Figure 2: Section through 3D sedimentary succession simulated by geological process model SedSimple over 5 Myr with five 1 Myr relative sea level cycles. A,B,C: Overall rising sea-level (A inset). D,E,F: Overall falling sea-level (D inset). A,D: Distribution of sedimentary facies. B,E: Water depth at time of deposition. C,F: Deposition time within each I Myr cycle.

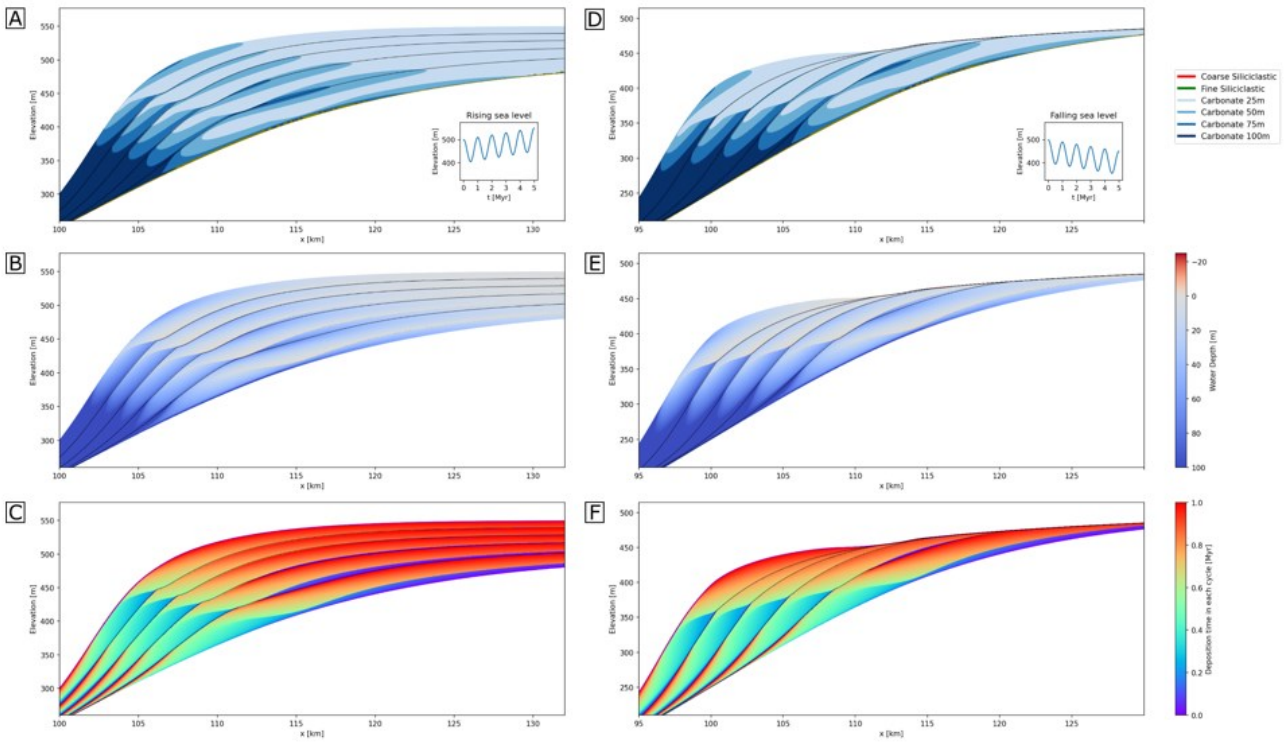

3. Results

3.1 Relationships between location, water depth, facies and depositional age

Landward-to-seaward cross sections through the two sequences are shown in Fig. 2, with Fig. 2A-C modelling rising sea level, and Fig. 2D-F falling sea level. For both scenarios, almost all of the rock volume on the slope comprises carbonate sediment (siliciclastics occupy only thin layers upon sequence boundaries), and the four carbonate facies are distributed in approximately similar patterns within each parasequence (Fig. 2A,D). These facies distributions correspond to changing water depth in which each was deposited (Fig. 2B,E), and time of deposition within each 1 Myr cycle of the final rock volume (Fig. 2C,F).

From these models, the trajectories of vertical elevation (vertical axis), depositional age (horizontal axis) and facies type (colours) of sediments preserved along six vertical transects that are geographically distributed across a cross-section from the seaward, deeper basin (transect 1) to the near shore (transect 6) can be derived (Fig. 3). The distribution of intervals of hiatus on each transect are shown as dotted horizontal sections on each curve (panels (b) in Figure 3A and 3B). Different parts of the relative sea-level curve are sampled in the overall rising compared to the falling sea-level scenarios. Both scenarios sample the start of the sequence boundary formation in the first cycle, but this may be an artefact produced by the initiation of the model run. After this, in the overall rising sea-level scenario, samples lie dominantly in the transgressive systems tract in all cycles, but with temporal coverage decreasing, and terminating at the MFS in most transects in later cycles. Most terminations correspond to parasequence boundaries observed in Fig. 2, with the onset of each hiatus starting within the latest transgressive systems tracts. In shallower transects these are approximately temporally coincident with the maximum flooding surface, and some extend into the highstand sequence tract.

In both simulations of overall rising and falling sea level, hiatuses span more than 50% of geological time on all but the seaward-most transect, and increase to 86% and 95% for the most landward transects in each simulation, respectively (Figs. 3A, 3B, panels c). The overall length of time recorded in the sedimentary succession is greater in the falling sea-level scenario since increased erosion of shallow sediments results in more continuous deposition in basinward transects, and in both scenarios the deepest transects contain the most complete temporal records.

Figure 3: **Cross-sections and vertical transects through 3D sedimentary succession simulated by geological process model SedSimple over 5 Myr with five 1 Myr sea level cycles.** A,C: Overall rising sea-level. B,D: Overall falling sea-level. a) deposition time within each I Myr cycle, with location of six vertical transects. b) distribution of facies deposited through time in each transect. Dotted horizontal sections of curves show hiatuses. c) total percentage of time missing (hiatuses) in each transect. MFS = Maximum Flooding Surfaces. C,D: a) deposition time within two 1 Myr cycles, with location of six vertical transects. b) distribution of facies in each transect through time. Dotted horizontal sections of curves show hiatuses. Regularly spaced geological time samples (red dots between 0.25 and 1 Ma) are projected (arrows) to elevations on each transect at which those times are recorded in the sedimentary record. Dashed arrows show time samples preserved on more than one transect. The distribution of projected points (small triangles in a) is the set of vertical transect sample points that represent regular sampling of geological time.

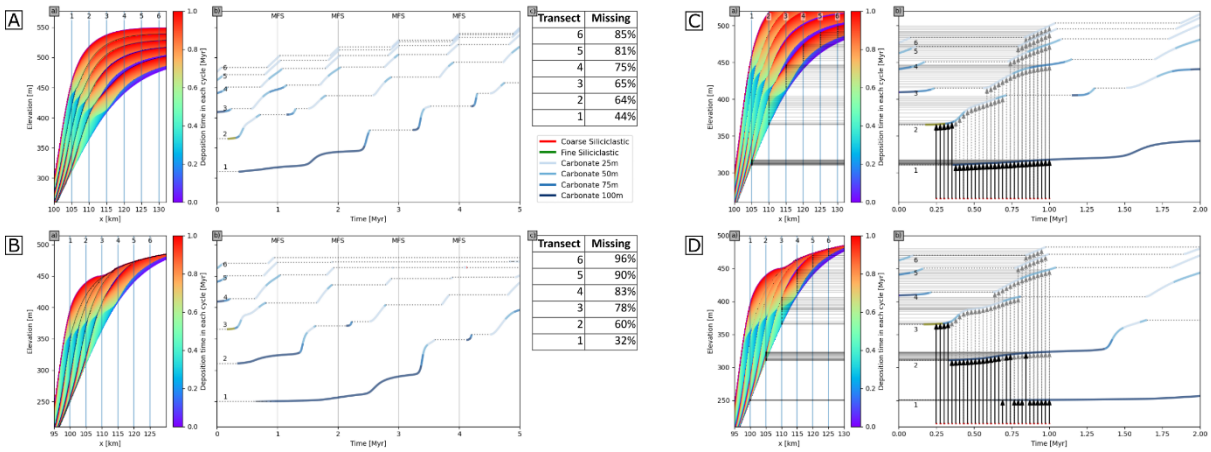

3.2 Implications for experimental design of geochemical sampling

Spatial samples that represent regular time intervals can be identified on each transect. Regular points spanning the period 0.4 to 1 Myr (red dots, Figs. 3C,D panels (b)) are projected upward to intersect the set of depositional trajectories (vertical arrows). If non-zero gradients are encountered in any trajectory, this indicates that sediment deposited at that time is preserved on the corresponding transect. Projecting such intersection points across to the elevation axis provides an exact location of the corresponding sample (horizontal arrows). Samples on other transects may also record the same point in time (dashed arrows).

Panels (b) in Fig. 3C,D show that regular samples of geological time are distributed unevenly in space on each transect (and by corollary, regularly-spaced sampling along any vertical transect represents geological time irregularly). The projected locations of those regular time samples represents an experimental design for spatial sampling along the set of transects that records geological time without bias. Many but not all times can be observed on multiple lateral transects, but there is no time that can be observed an all transects.

The abundance of hiatuses with significant and variable duration in vertical sampling transects creates difficulties for the temporal interpretation of recorded data if environmental conditions and hence geochemical proxies vary temporally (secularly), laterally (spatially) or both. Systematic and highly variable carbonate $\delta^{13}C$ values can occur in different, but time-equivalent, facies, which in turn are used to infer regional or global scale stratification of $\delta^{13}C$ with water depth (e.g., Kump, 1991). We recognise that some of the proximal-to-distal differences seen in $\delta^{13}C$ records may be diagenetic in origin, or caused by differing fractions of transported (e.g. neritic versus pelagic) material, and so would not reflect the isotopic composition of the water column. Nevertheless, these processes themselves may also have a depth-dependent control, as shown by Ediacaran examples (Busch et al., 2022; Lu et al., 2013). So here we simply explore the effects of sampling as used to attempt to constrain this gradient, and then test the effect of a $\delta^{13}C$ water column gradient on the resultant modelled records.

Geochemical gradients of $\delta^{13}C$, as well as redox gradients inferred from redox-sensitive trace element concentrations and isotopes in the water column, can only be constrained if signature variations of contemporaneously deposited samples from different water depths are available (Lu et al., 2013; Yuan et al., 2023). This requires samples from laterally offset locations identified by sequence stratigraphic analysis. If either the gradient or the overall

environmental signature varies secularly, panels (b) in Fig. 3 show that some time intervals contain insufficient data to constrain the gradient, with only one or even no samples preserved.

Water depth at time of deposition varies significantly within, and between, different vertical transects (Figure 4). Using the example gradient of (Giddings and Wallace, 2009), insertion of a $\delta^{13}C$ axis creates significant scatter in the resultant $\delta^{13}C$ values (Fig. 4, panels b). If water depth is not known, data from samples deposited in different water depths are usually combined without correcting their measured signatures to a common water depth datum, so this scatter obscures the signature of true, secular environmental change (environmental conditions, represented by the chemical gradient in the water column, are temporally constant in these simulations).

If recorded seawater geochemical signatures change both with relative water depth (spatially, synchronously) due to vertical chemical gradients, and secularly (temporally) due to environmental dynamics, then these spatiotemporal effects may be confounded in recorded data. Here we further analyse results with these effects separated, revealing concomitant issues for regional and global correlation of geochemical signatures.

Figure 4: Sections through 3D sedimentary succession showing water depth changes simulated by geological process model SedSimple over 5 Myr with five 1 Myr sea level cycles. A: Overall rising sea-level. B: Overall falling sea-level. a) Water depth of deposition within each 1 Myr cycle, with locations of six vertical transects colour coded. (b) Water depth and $\delta^{13}C$ values in each (colour coded) transect through time, assuming gradient shown on left vertical axis. Grey lines show full water depth history along each transect.

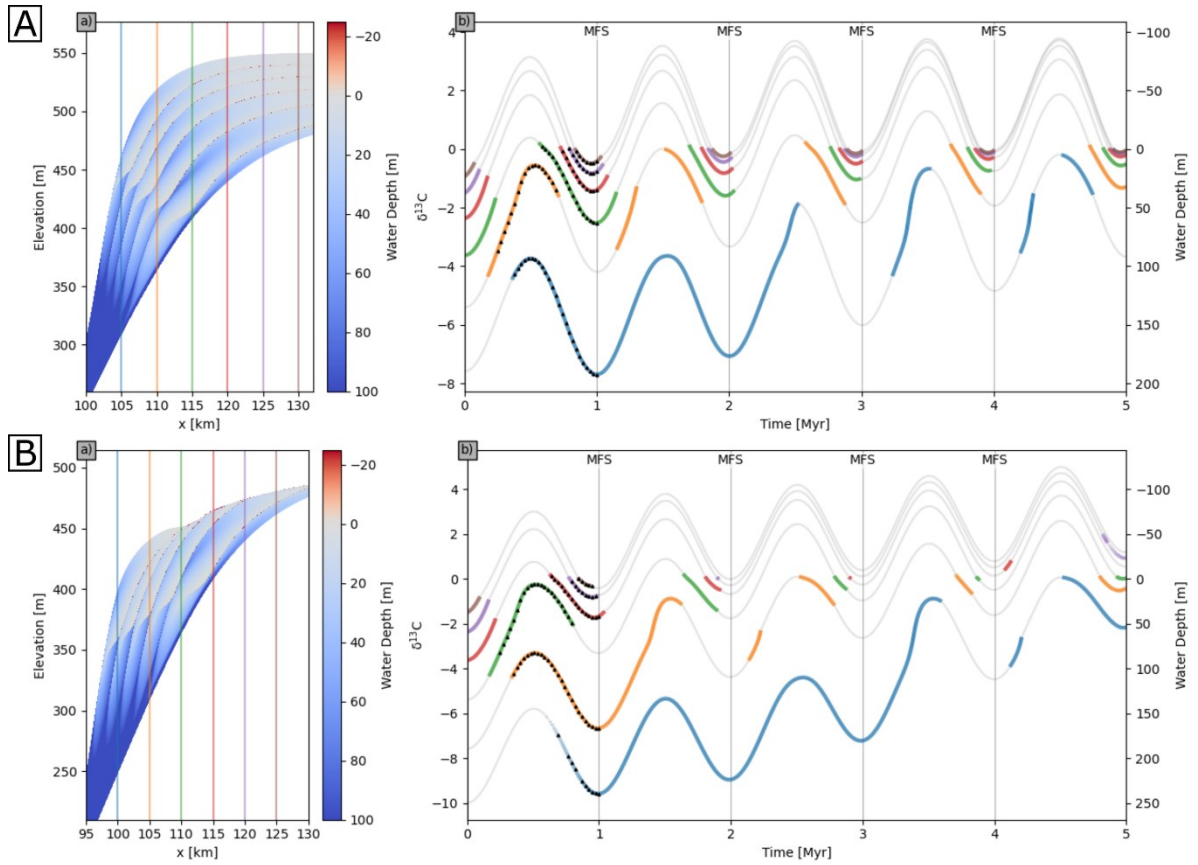

3.3 Spatial geochemical gradients with water depth; no secular variation

The distribution of vertical lithologies can be combined with their modelled $\delta^{13}C$ values for each transect, in overall rising (Figure 5), and falling (Figure 6) sea-level models. These are displayed both as vertical transects in space as might be derived from core or outcrop (log height: Figs. 5A, 6A) and after interpolation to time (Ma: Figs. 5B, 6B) (See Methods, sampling transects).

Figure 5: $\delta^{13}C$ values in overall rising sea-level scenario. A: Derived from six transects (a to f; colour coded as in Fig. 4), and all combined (g), plotted by height in a 3D sedimentary succession simulated by geological process model SedSimple over 5 Myr with five 1 Myr cycles, assuming $\delta^{13}C$ gradient shown in Figure 4. B: $\delta^{13}C$ values in A linearly interpolated to time assuming that recorded data span the complete 5 Myr interval, with correct temporal record of preserved sediments shown in black.

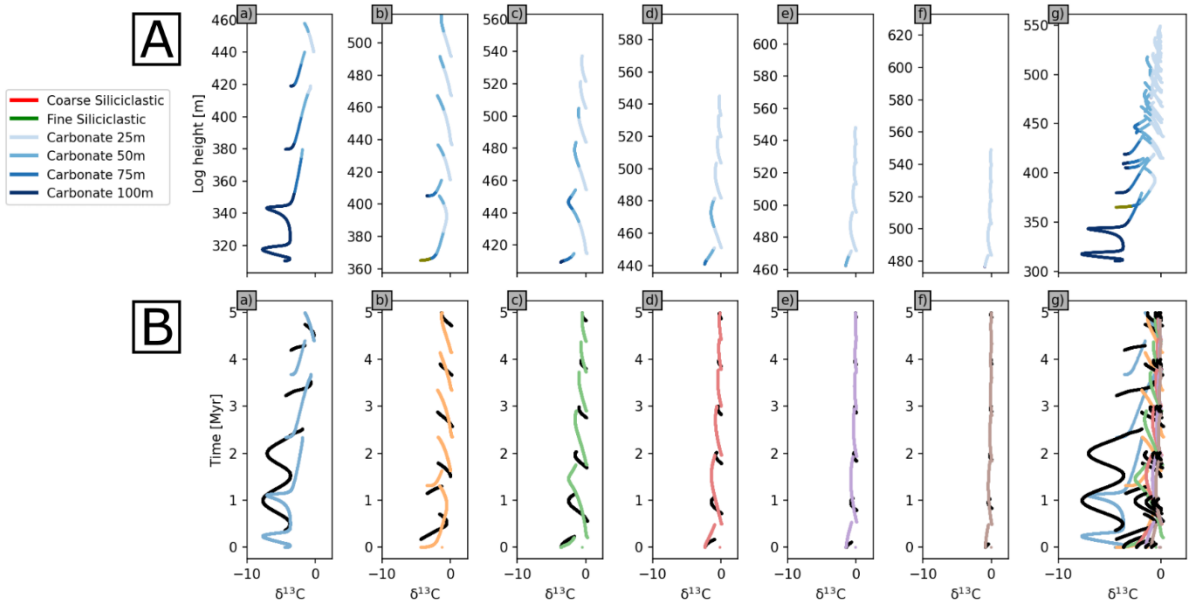

Figure 6: $\delta^{13}C$ values in overall falling sea-level scenario. A: Derived from six transects (a to f; colour coded as in Fig. 4), and all combined (g), plotted by height in a 3D sedimentary succession simulated by geological process model SedSimple over 5 Myr with five 1 Myr cycles, assuming $\delta^{13}C$ gradient shown in Figure 4. B: $\delta^{13}C$ values in A linearly interpolated to time assuming that recorded data span the complete 5 Myr interval, with correct temporal record of preserved sediments shown in black.

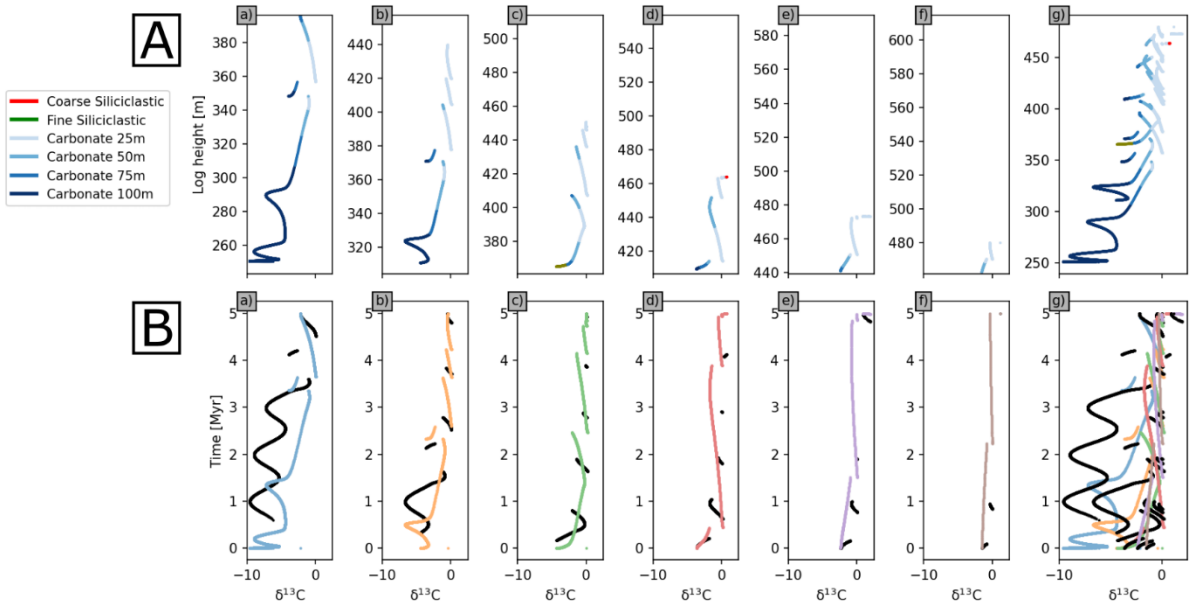

Even with secular variations in environmental conditions excluded, modelled vertical transects show highly variable signatures that track relative water depth changes, with many step-like offsets due to hiatuses. Combined data on a single scale of vertical elevation show that offsets are highly variable in elevation (Figs. 5A(g), 6A(g)). Figs. 5B, 6B compare the correct temporal record of $\delta^{13}C$ values of preserved sediments (shown in black) to the spatial transects in panels A after linear interpolation to time assuming that the recorded data spans the complete 5 Myr interval (shown in colours), i.e. assuming that dateable beds (5 Myr and 0 Myr) lie at the top and bottom of the succession. The fragmentary and condensed nature of the record is clear in all transects, but is most striking in the shallowest realms. These characteristics of the temporal record are highlighted when data from all transects are combined (Figs. 5B(g), 6B(g)).

It is notable that the magnitude of $\delta^{13}C$ variability is far greater in deeper transects, approximately six times greater in panels (a) than panels (f) in Figs. 5 and 6. This is because shallower transects sample only short sections of each cycle, and these sections span similar ranges of cycle phase and hence water depth (Fig. 4). Since water depth controls $\delta^{13}C$ variability, sampling the same depth in each cycle results in a relatively homogeneous signature along shallow transects.

It is not possible to interpolate the spatial logs to the correct temporal logs by linear stretching unless variable hiatuses are inserted across every data offset. However, even with our continuous (infinitely finely sampled) vertical logs, it is hard to identify the position of those data offsets in shallower transects. Given discretely sampled and noisy field data this

would likely be impossible. It is therefore effectively impossible to perform correct interpolation to time on individual logs without additional constraints on hiatuses.

3.4 Implications for basinal correlation

In principle, constraints on hiatuses in one transect are available from data on other transects which span a portion or all of each hiatus of interest. This requires that logs from different transects are placed correctly on a common time axis; a basic requirement is therefore that the representation of each stratigraphic cycle can be correctly correlated between transects. The fragmentary and highly variable nature of these records poses a challenge for intra-basinal correlation.

To explore this, an experienced stratigrapher interpreted sequence boundaries, and shallowing-up (regressive) and deepening-up (transgressive) packages (see Methods, Correlation exercise), further providing written justification (see Supplementary Materials). In transects through the model with overall rising sea-level, the match between interpreted and modelled correlations of sequence boundaries and packages is exact for transects (c) to (f), but incorrect for the deepest transect (a), and in part for (b) (Fig. 7A,B). However, in the model with overall falling sea-level the match is generally poor, with a widespread mismatch of sequences (Fig. 7C,D). This disparity between reality and results from commonly applied interpretational methods and essentially perfect data, highlights a widespread issue which is likely compounded when considering discretely sampled spatial data points subject to various sources of experimental errors, and inter-regional transects to produce global temporal correlations.

Figure 7: $\delta^{13}C$ values and facies distribution derived from six transects (a to f) plotted by height through a 3D sedimentary succession, simulated by geological process model SedSimple over 5 Myr with five 1 Myr sea level cycles, assuming the $\delta^{13}C$ gradient shown in Figure 4. A,B: overall rising sea-level; C,D: overall falling sea-level. A,C: Interpreted correlation from an experienced stratigrapher; B,D: Correct correlation. Appendix B provides the interpreter's narrative justification for interpreted correlations.

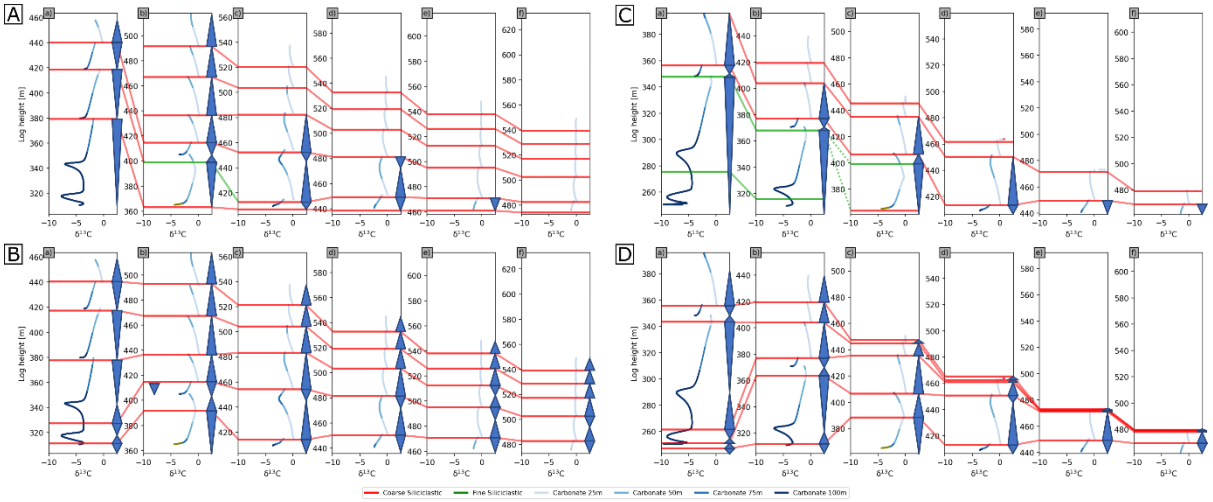

3.5 Secular geochemical changes; no gradient with water depth

An important consequence of our results is that due to the large intervals spanned by hiatuses (Fig. 3), there is a greater than 50% probability that landward transects will not preserve any short-lived event, such as the geochemical consequences of a large volcanic eruption, at all. Very short-lived geochemical phenomena are therefore not likely to provide robust signals to correlate between such transects.

We now consider three frequencies of continuous secular change in seawater composition, of one, two and four cycles in 5 Myr, with an amplitude of 8‰ with no gradient with water depth. Simultaneously, sea level varies as in previous simulations.

Rising sea-level: Fig. 8 shows logs in height, and the same data interpolated to geological time across the six transects for an overall rising sea level. Similarly to the case with geochemical gradients with respect to seawater depth, basinward transects record substantially more of the temporal record than landward transects, and multiple hiatuses result in large data offsets in all logs. Sampling of time is so sparse in shallow water successions that a clear aliasing effect occurs: in Fig. 8F panels (b) to (f), four true secular oscillations result in a single, lower frequency apparent oscillation in the temporal log (dashed red line, panel (f)).

Falling sea-level: For the case of overall falling sea level the record is far less well-sampled than for the rising sea level case (Fig. 9). The most continuous records are again basinward, yet even there the true secular change is variably condensed and expanded in space or time so as to make it extremely difficult to recognise the true secular cyclicity, even for the lowest frequency case (Fig. 9F). If data were sampled at regular intervals as is currently standard in the field, many data in these logs would likely be dismissed as scatter.

Figure 8: $\delta^{13}C$ values and facies distribution. Derived from six transects (a to f), and all combined (g) by depth through 3D sedimentary succession simulated by geological process model SedSimple over 5 Myr with an overall rising sea-level and five 1 Myr cycles, assuming no $\delta^{13}C$ gradient but three secular changes of $\delta^{13}C$ as shown in insets, by A, depth; B, in time, with correct temporal record of preserved sediments shown in black, and full model spatial output (A) linearly interpolated to time assuming that the recorded data spans the complete 5 Myr interval. Panel F(f) shows apparent cyclicity due to aliasing (dashed red).

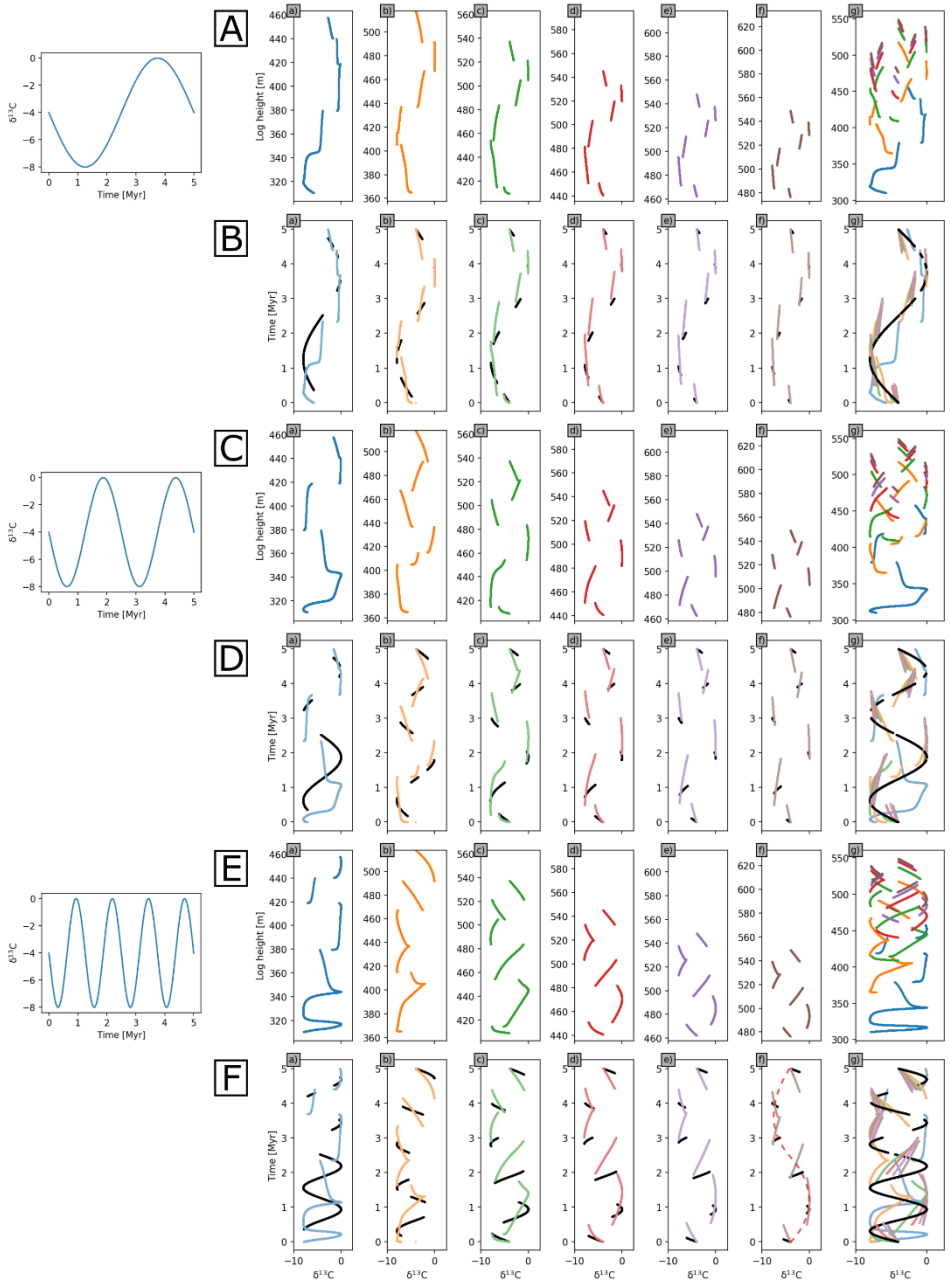

Figure 9: $\delta^{13}C$ values and facies distribution. Derived from six transects (a to f), and all combined (g) by depth through 3D sedimentary succession simulated by geological process model SedSimple over 5 Myr with an overall falling sea-level and five 1 Myr cycles, assuming no $\delta^{13}C$ gradient but three secular changes of $\delta^{13}C$ as shown in insets, by A, depth; B, in time, with correct temporal record of preserved sediments shown in black, and full model spatial output (A) linearly interpolated to time assuming that the recorded data spans the complete 5 Myr interval. Panel F(f) shows apparent cyclicity due to aliasing (dashed red).

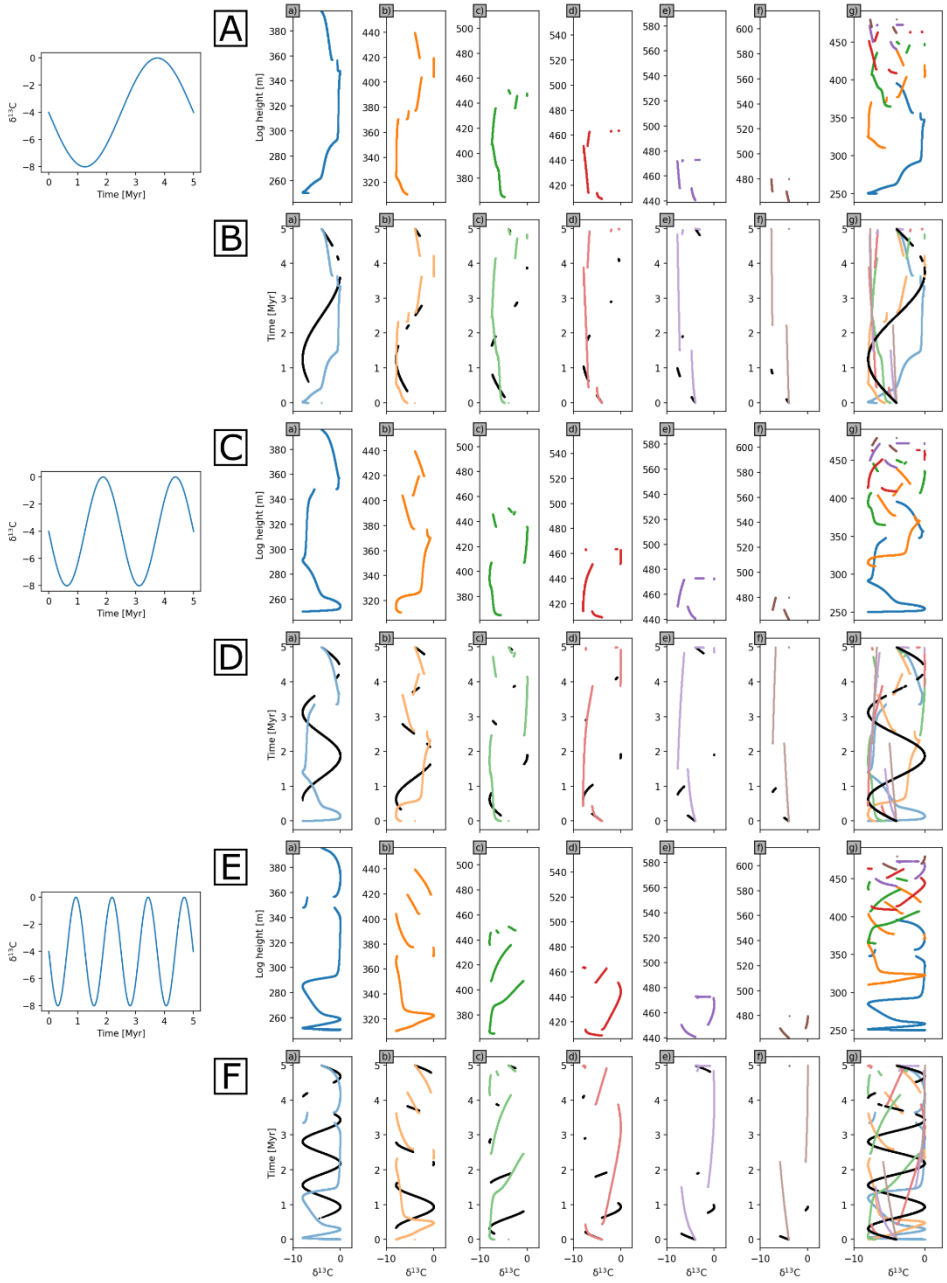

3.6 Aliasing and Nyquist's theorem

An aliasing effect occurs because temporal sampling along the transects in shallow successions violates Nyquist's theorem, which states that more than two samples per oscillation (the Nyquist sampling frequency) are needed in order to record any oscillating signal unambiguously (Shannon, 1949). Whenever sampling is less dense than the Nyquist frequency, the true oscillation frequency (e.g. Fig. 8F) is irreversibly expressed as a signal at a lower *apparent* frequency (the red dashed curve in panel (f)). Since in shallow records only one short section of each cycle is recorded rather than two (Fig. 4, panels (b)), there is what we might call a *natural* sampling interval (the reciprocal of the corresponding natural sampling frequency) approximately equal to the period of sea level oscillations. Geochemical data therefore contravenes the Nyquist criterion.

If the parasequence (sea level) oscillation period is τ then its frequency is $f_\tau = 1/\tau$. We effectively obtain one sample per oscillation in Fig. 4, so the Nyquist sampling frequency is $f_N = 1/(2\tau)$. Say the true secular oscillation in geochemistry has period T (frequency $f_T = 1/T$). Given the samples in Fig. 4, Nyquist's theorem states that the true frequency f_T appears instead to have the apparent frequency $f_A = |2n f_N - f_T|$, where n takes whatever integer value gives a result that lies within the range $-f_N$ to $+f_N$. This means that *all* true secular variations at frequency higher than f_N in the geochemical data are projected into significantly lower apparent frequencies. In Fig. 8F, sea level oscillates with period 1 Myr, seawater geochemistry oscillates with period 1¼ Myr, and Nyquist's formula above predicts an apparent frequency $f_A = 1/5$ cycles per Myr (or one cycle per 5 Myr), which is exactly that observed in Fig. 8F(f).

The similarity in shape between the signatures observed in rows B and F in Fig. 8 is therefore a result of aliasing. If a true secular change similar to that in row B occurred in one

interval of time, and that in row F occurred in another, observed geochemical signatures would appear to be very similar such that these two intervals might be correlated erroneously. For any logs other than the two most basinward, it is therefore extremely difficult to interpret the true secular oscillation period of 1.25 Myr in Fig. 8F, even given perfect (spatially continuous) log data along each transect. The Nyquist sampling violation is likewise visible in the falling sea-level scenario (Fig. 9F), particularly in panels (c), (d), (e) and (f) in row F, which appear to embody at most 3, 2½ , 1 and 1 oscillations, respectively.

4. Discussion

We use model simulations to quantify where in space and time standard geochemical (or paleontological) sampling techniques fail to sample adequately, and how they could be improved. Even in simple relative sea level scenarios with no secular geochemical change, sampling deficiencies lead directly to false temporal correlations between locations. The effects of relative sea level variations (which include both the effect of absolute sea level change and subsidence) combined with either chemical gradients with depth, or secular chemical variation, are also shown to impact signatures and interpretations of standard geochemical logs under apparently reasonable assumptions of past environmental conditions. Nevertheless, some scatter in logs from marine basin environments may be understood systematically by deploying sequence stratigraphic concepts. One implication is that current methods of both sampling procedures, and temporal interpretation of geochemical logs, may require modification.

4.1 Examples of biases from chemostratigraphic data

Our results show that the principle factor challenging the correlation of disparate transects is the amount of time missing at unconformities. Since hiatuses span from 50% to 95% of geological time on all but the seaward-most transect, the fragmentary and condensed nature of the record is clear in any vertical transects, but is most striking in the shallowest realms. Regular geochemical sampling along any vertical transect samples geological time highly irregularly, with each well sampled period potentially followed by a long hiatus; this pattern may be repeated in each cycle. These results demonstrate that the fragmentary nature and under-sampled nature of these records poses a challenge for intra-basinal and global temporal correlations: there is a greater than 50% probability that landward transects will not preserve any short-lived event, preventing their correlation between transects. The extent of the outlined biases can only truly be determined by a close examination of published geochemical datasets in their stratigraphic context.

Here we outline some examples from the geological record where such biases and phenomena may be present. Particular care needs to be paid to the identification of, and sampling through sequence boundaries, due to likely missing or condensed sedimentary records, even in deeper settings. Where events have been recognised and adequately resolved, variable sedimentation rates may nonetheless microscope or telescope time alternately, if stratigraphic thickness is equated to duration. There are numerous examples in the literature of carbon isotope excursions, for example, that coincide with major eustatic sea level rise, in which case we would predict an abrupt initial change (the 'event'), followed by a more extended return (the 'recovery') to the long-term norm. Gradual geochemical shifts during transgressive episodes may thus erroneously be interpreted as rapid events, as they are likely to be associated with decreased sedimentation rates. Examples of this can be seen perhaps at the Cenomanian-Turonian boundary, which in some sections is characterised by an abrupt

positive $\delta^{13}C$ excursion (e.g., Jarvis et al., 2006), but in others by a more symmetrical hump (Li et al., 2017). Although students of geology know that time is unlikely to be expressed proportionately in vertical section, this is still commonly assumed, leading to interpretations of unusually rapid or near instantaneous perturbation, e.g. in $\delta^{44/40}Ca$ values (Du Vivier et al., 2015; Husson et al., 2015a). In such cases, the recognition of astronomical cycles through expanded sections commonly reveals that rapidly changing $\delta^{13}C$ values are expressed within an interval of anomalously thin cycles. In the case of the Cenomanian-Turonian event, such cyclostratigraphy has revealed that the carbon isotope recovery phase, far from being more gradual, was in reality more rapid than the "event" itself (Li et al., 2017).

Similar issues may be found with events for which there is at present inadequate time resolution, for example Precambrian events, such as the late Ediacaran 'Shuram' anomaly. The Shuram excursion is one of the largest negative carbon isotope excursions of the entire geological record. It has been reported from many regions of the world (Husson et al., 2015b; Lu et al., 2013), but is commonly described as asymmetric, describing an abrupt downturn followed by a gradual recovery. However, although widely recognised as coincident with major sea level rise (Busch et al., 2022), and therefore considered to be condensed at its base (Grotzinger et al., 2011), the Shuram excursion is still frequently described as being a "rapid" event, followed by a "gradual" recovery. Loose mixing of temporal and spatial terminology is commonplace, but if believed can lead potentially to unrealistically catastrophic interpretations (Bergmann et al., 2022) of what might have been relatively gradual system change. Indeed the shape of the Shuram anomaly varies greatly due to variable sedimentation rates even within the same sedimentary basin (Lu et al., 2013) and with the presence of unconformities (e.g., Husson et al., 2015b).

Our models show that the magnitude of $\delta^{13}C$ variability is far greater in deeper transects (Figures 5 and 6). This can often be seen in the published record of isotopic events (e.g., Wang et al., 2016). But as carbonates may be rarer in deeper settings (before the Mesozoic), this may not always be evident, or may only be recorded by the organic carbon isotope record, which can be more ambiguous due to isotopic fractionation during microbial reworking of organic matter. Deeper transects can be seen to record more time, capturing more complete trends related to vertical gradients, sea level cyclicity and secular variation in seawater. However, distal realms may also become sediment-starved, necessitating closer sampling. An example of this can be seen in studies of the lower Jurassic, in which different sections exhibit expanded records at different times (Bodin et al., 2023). Variable proportions of neritic versus pelagic components further complicate the situation, leading to the absence of excursions in some transects, or even modest positive excursions in shallower transects being coeval with modest negative excursions in more distal realms. Such time-equivalent discrepancies may be caused when the magnitude of secular change is less than the vertical (neritic versus pelagic) isotopic gradient, and so can be overprinted by changes in carbonate transport into more distal realms. In cases of major anomalies though, the notion that deeper settings reveal a truer picture is frequently confirmed in lower Paleozoic studies, for example, whereby more basinal settings reveal larger, and more complete excursions (Schiffbauer et al., 2017). In some cases, the organic carbon isotope record may be the only dataset available for correlation, and can present a far more apparently smooth record in deeper settings than the highly discontinuous carbonate carbon isotope record (Bodin et al., 2023). Although frequently done, labelling transects or stratigraphic units by depth (e.g. shallow/deep rather than proximal/distal) throughout their thickness can be misleading, and ought to be avoided in favour of following trajectories of change through specific facies (see Busch et al., 2022,

Fig. 6). In practice, this may be very difficult to do in detail, and so it should be borne in mind that depth gradients, and changing sea level, impact even seemingly "deep" transects.

Shallower realms are affected disproportionately by sea-level falls, leading to missing stratigraphy and incomplete or absent isotopic events. A good example of this is the lower Cambrian, which is characterised by a succession of quite extreme carbon isotope and other geochemical perturbations (Maloof et al., 2010). In cases where shallower transects record more highly resolved cyclicity, this may be a sign that carbonate production rates during an isotopic excursion have kept pace with synchronous (eustatic) sea level change (Schiffbauer et al., 2017), potentially indicating a causal connection to the global carbon cycle. As carbonate production rates are highest in shallow settings, accommodation needs to be created at higher rates in such settings in order to preserve more complete records. In the case of the Cambrian carbon isotope record, missing excursions due to emergence and consequent erosion as well as sediment starvation and phosphogenesis have led to numerous labelling schemes, and ambiguous correlations, which have needed to be updated continually over the past 40 years (Bowyer et al., 2022). Although a popular practice, excursion numbering, rather than naming, is destined to become confusing as ever more highly resolved, and potentially less aliased records become available.

The effects of under-sampling are clearly observed in Fig. 10, which shows $\delta^{13}C$ values and respective lithologies from a high resolution, sub-vertically sampled transect through an Ediacaran mixed carbonate-clastic ramp succession (Omkyk member, Nama Group, Namibia), spanning five high-frequency cycles, where every distinct lithological bed was sampled. While complex, highly variable patterns are observed in the data set (small blue circles), a clear overall signature consisting of almost two full oscillations with a wavelength of around 3m is observed, which is resolvable using samples separated by an interval of around 0.7 m (dashed line, panel A). This is replaced by a spurious signature consisting of a

single oscillation with an apparent wavelength >5 m if the inter-sample interval is reduced to 1.2 m or 1.6 m (panels B,C), similarly to the aliasing example discussed above.

Figure 10: $\delta^{13}C$ values and respective lithologies from a sub-vertically sampled, mixed carbonate-siliciclastic ramp succession at Omkyk, Ediacaran Nama Group (Omkyk Member), Namibia, sampled in every distinct lithological bed at irregularly spaced intervals and showing the position of five high-frequency cycle boundaries. Data points that would have been sampled at approximately regular 0.7 m (A), 1.2 m (B), and 1.6 m (C) intervals are highlighted as large circles and joined by dashed lines.

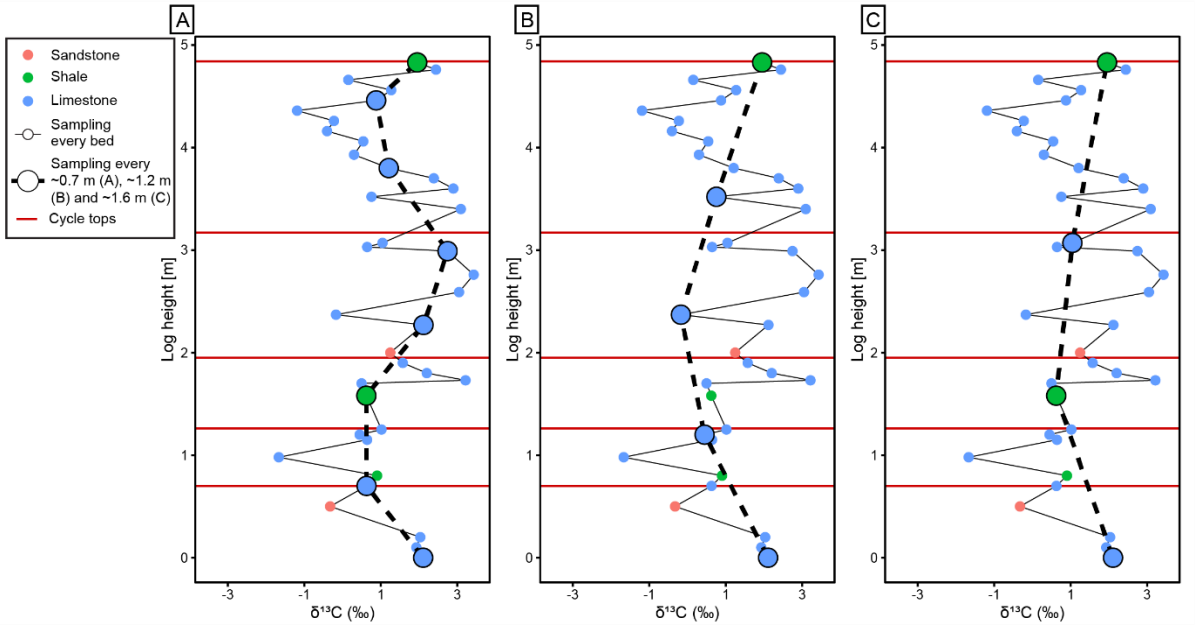

4.2 Irreversible aliasing of the shallow marine record

Aliasing is likely to occur in many datasets consisting of proxy values sampled along individual transects. Oscillatory signals with geographically and temporally varying amplitudes are often caused by Milankovitch cycles (Imbrie, 1985). These occur on a variety of frequencies, some of which oscillate significantly more rapidly than the Nyquist frequency of field data sets and so will be aliased. In addition, any process that repeatedly perturbs an equilibrium state of a model and then returns to equilibrium may create significant oscillatory

components in proxy data that again operate on a variety of timescales which may exceed the Nyquist frequency (von der Heydt and Ashwin, 2016).

From a theoretical point of view, there are a number of ways in which aliasing of time series can be reduced: (i) sampling regularly in time at a higher density of points increases the Nyquist frequency so that higher frequencies can be observed unaliased; (ii) observing the n^{th} order temporal derivatives of the signature of interest at each point, in addition to the signal value itself, multiplies the Nyquist frequency by $n+1$; or (iii) applying an anti-alias filter, which removes the higher frequencies from the data, prior to or during the measurement of proxy data values.

In principle, sampling more densely in space along transects resolves time in the rock record at higher spatial resolution. However, this provides no extra data at times of hiatus so it is not possible to sample *regularly* more closely than the natural sampling interval. Thus, strategy (i) fails.

In principle, strategy (ii) can be tested: instead of one sample at each location, two or more very closely-spaced samples can be taken, separated by a spatial interval dz corresponding to time interval dt that is sufficiently small that geological dynamics have not changed between samples. The first order temporal derivative is approximated by a finite-difference formula, $p'(t+dt/2) = [p(t+dt) - p(t)]/dt$ where $p(t)$ is the proxy value at time t, and if a cluster of more than two samples are taken at regular intervals dt then higher-order derivatives are estimated by applying this formula recursively (e.g., second-order derivatives (curvature) are approximately $p''(t+dt/2) = [p'(t+dt) - p'(t)]/dt$. However, estimating dt from dx is our ultimate goal. By the law of superposition $dt > 0$ so the sign (+ or -) of derivatives will be observed correctly, but their magnitude scales with $1/(dt)^n$ which will be in error. Errors may be compounded by consideration that dt must be greater than the residence time of the

geochemical or other proxy being explored, otherwise signatures of sample pairs are not independent. And finally, the absolute time t for each sample cluster remains unknown *a priori* due to the presence of hiatuses between sample groups.

Strategy (iii) involves removing aliased frequencies from proxy data prior to or during sampling or measurement. One possibility is to use samples or proxies for which Earth processes have already damped or removed the signatures of all dynamics that act at frequencies higher than half of the natural sampling frequency (i.e., than the Nyquist frequency). For example, say the inter-sample interval is equal to the residence time of the proxy: assuming that the proxy already averages-out variations due to processes that occur on shorter timescales (higher frequencies), aliasing effects would be removed. Since it is not possible to sample both regularly and more densely than the natural sampling interval τ, we require the proxy residence time T_p to be at least as long as the natural sampling interval. Any dynamic process that controls proxy signatures on timescales shorter than the natural sampling interval, yet longer than the proxy residence time, remain aliased.

Aliasing might be *detected* using derivatives. The temporal derivative of signatures (slope of black line segments) are observable in Figs. 8 and 9. Using only the sign of each gradient (observable from closely spaced samples) it is clear that some indicate a local slope that goes counter to the slope of the apparent (aliased) oscillation – compare the slope of each black line segment with the corresponding slope of the dashed red curve in Fig. 8F, panel f. This indicates that the data include a higher frequency signal with peaks or troughs between each pair of sample points, and therefore that aliasing has occurred.

Aliased frequencies can then be further constrained using a variant of strategy (ii). The highest possible frequency of signal resolvable by the proxy is $f_p = 1/T_p$, since the proxy would average higher frequency oscillations approximately to zero. The aliased signal must

therefore lie in the range $[f_N, f_p]$. Estimating the geological age of each sample is still a non-unique inverse problem to be solved, e.g., using computational methods such as in (32,33), but even only the signs of spatial (and hence, temporal) derivatives of proxy data place constraints on those ages.

Finally, Nyquist's theorem implies that aliased frequencies depend only on the frequencies of secular and sea level variations; estimates of these quantities allow aliased frequencies to be predicted. E.g., in Fig. 9 we might assume that sedimentologically observed hiatuses indicate 5 sea level oscillations between ages 0Ma and 5Ma so on average τ=1Ma and f_τ = 1Ma^{-1}, while signs of derivatives on the deepest transects indicate all secular oscillations, in this case 4 oscillations giving an average T=1.25Ma and frequency f_T = 0.8. As above, Nyquist's theorem correctly predicts an apparent frequency f_A = 1/5Ma^{-1}.

Thus we predict how the true geochemical secular frequency observed on the basinward transect will be expressed on the shallowest transect. Careful field observations thus allow the low-frequency aliased signal (Fig. 8, lower-right) to be correlated correctly with the higher-frequency unaliased signal (lower-left).

5. Conclusions

Most current studies identify geochemical events that would then be correlated to similar features in other records, initially within the same basin, but eventually worldwide if applicable for that proxy. We show that sampling in this way could introduce bias into the measured proxy record, obscuring or overprinting the true record of secular change even with infinitely dense sampling. Our simulations find that hiatuses are substantial in all but the deepest sections, and span from 50% to 95% of geological time as we move landwards. The time series distortions explored above, caused by vertical water-depth gradients and

oscillating sea level, have predictable consequences for sedimentation rate and platform erosion. These interacting effects may delete, diminish or exaggerate isotopic events, even producing apparent events when there were none. Indeed, there is a greater than 50% probability that landward transects will not preserve any short-lived event, and so will also preclude any correlation of such events between deep and shallow transects. Finally, we show that the geological sampling of time is so sparse in landward successions that a clear aliasing effect of secular changes occurs: higher resolution secular oscillations result in a single, lower frequency apparent oscillation in the temporal log.

Regular geochemical sampling along any vertical transect, but most problematically in shallow successions, will therefore not only contain a succession of hiatuses of unknown number and duration, but will also sample geological time highly nonlinearly. This is demonstrated to cause substantial errors in correlation between sub-vertical sampling transects along which environmental (e.g., geochemical) data are recorded, particularly in falling sea-level scenarios. Geochemical gradients in the water column can only be constrained if signature variations of contemporaneously deposited samples from different water depths are available. If either the gradient or the overall environmental signature varies secularly, some intervals will always contain insufficient data to constrain the gradient. Both geological process model SedSimple and published geochemical data provide evidence for substantially more complex stratigraphic relations than are commonly assumed in deep-time paleo-environmental analysis.

Hiatuses may be stratigraphically controlled, and so follow semi-regular spatio-temporal patterns. This property masks true secular environmental changes, in some cases causing higher frequency environmental variations to be aliased (transposed) to appear as lower-frequency spurious signatures. Such effects may be detectable by sampling more densely than is normally assumed sufficient. However in many cases aliasing will be undetectable, and it is

likely that in many shallow marine settings where sea level fluctuations are significant its effect is irrecoverable; this implies that widespread adoption of formal and robust uncertainty assessment in paleo-environmental interpretations is of critical importance.

Acknowledgements

Funding: RW and FB thank UKRI Project NE/T008458/1 for funding support. AC and HB acknowledge funding from the Edinburgh Imaging Project sponsors, Total plc and bp plc. **Author contributions**: Conceptualization: AC. Methodology: AC, DT, HB. Investigation: HB, DT, AC. Visualization: HB, AC, RW. Writing—original draft: AC. Writing—review & editing: RW, FB, HB, GS, YZ, DT. **Competing interests**: Authors declare no competing interests; **Data and materials availability**: All new data are available in the supplementary material. For the purpose of open access, the authors have applied a Creative Commons Attribution (CC BY) licence to any Author Accepted Manuscript version arising.

References

Bergmann, K.D., Osburn, M.R., Wilcots, J., Cantine, M., Grotzinger, J.P., Fischer, W.W., Eiler, J.M., Bonifacie, M. 2022. The Shuram excursion: a response to climate extremes at the dawn of animal life. Authorea Preprints.

Bodin, S., Fantasia, A., Krencker, F. N., Nebsbjerg, B., Christiansen, L., Andrieu, S. 2023. More gaps than record! A new look at the Pliensbachian/Toarcian boundary event guided by coupled chemo-sequence stratigraphy. Paleogeog., Paleoclimatol., Paleoecol., 610, 111344.

Bowyer, F.T., Zhuravlev, A.Y., Wood, R., Shields, G.A., Zhou, Y., Curtis, A., Poulton, S.W.,

Condon, D.J., Yang, C. , Zhu, M. 2022. Calibrating the temporal and spatial dynamics of the Ediacaran-Cambrian radiation of animals. Earth-Sci. Revs., 225, p.103913.

Burgess, P.M., Wright, V.P. 2003. Numerical forward modelling of carbonate platform dynamics: An evolution of complexity and completeness in carbonate strata. Jour. Sediment. Res. 73, 637–652.

Busch, J.F., Hodgin, E.B., Ahm, A.S.C., Husson, J.M., Macdonald, F.A., Bergmann, K.D., Higgins, J.A. Strauss, J.V., 2022. Global and local drivers of the Ediacaran Shuram carbon isotope excursion. EPSL, *579*, p.117368.

Catuneanu, O., Abreu, V., Bhattacharya, J.P., Blum, M.D., Dalrymple, R.W., Eriksson, P.G., Fielding, C.R., Fisher, W.L., Galloway, W.E., Gibling, M.R., Giles, K.A. 2009. Towards the standardization of sequence stratigraphy. Earth-Sci. Revs., 92, 1-33.

Du Vivier, A.D.C., Jacobson, A.D., Lehn, G.O., Selby, D., Hurtgen, M.T., Sageman, B.B. 2015. Ca isotope strastigraphy across the Cenomanian-Turonian OAE2: Links between volcanism, seawater geochemistry, and the carbonate fractionation factor. EPSL, 416, 121-131.

Eichenseer, K., Sinnesael, M., Smith, M. R. & Millard, A. R., 2023. Dating the first Siberian trilobites with a Bayesian, stratigraphic age model. Tech. Rep., Copernicus Meetings.

Giddings, J. A., Wallace, M. W. 2009. Facies-dependent $\delta^{13}C$ variation from a Cryogenian platform margin, South Australia: Evidence for stratified Neoproterozoic oceans? Paleogeog., Paleoclimat., Paleoecol., 271, 196-214.

Grocke, D.R. 2020. Carbon isotope stratigraphy: Principles and applications. Stratigraphy & Timescales, Volume 5, 1-40.

Grotzinger, J. P., Fike, D. A., Fischer, W. W. 2011. Enigmatic origin of the largest-known carbon isotope excursion in Earth's history. Nat. Geo., 4, 285-292.

Hay**,** C.C., Creveling, J.R., Hagen, C.J., Maloof, A.C., Huybers, P. 2019. A library of early

Cambrian chemostratigraphic correlations from a reproducible algorithm. Geology, 47, 1–4.

Hill, J., Tetzlaff, D., Curtis, A., Wood, R., 2009. Modeling shallow marine carbonate depositional systems. Comput. Geosci., 35, 1862–1874.

Holland, S. M. 2023. The contrasting controls on the occurrence of fossils in marine and nonmarine systems. Bollettino della Società Paleontologica Italiana, 62, 2023, 1-25.

Holland, S. M., Patzkowsky, M. E. 1999. Models for simulating the fossil record. Geology, 27, 491-494.

Holland, S.M., Patzkowsky, M.E. 2015. The stratigraphy of mass extinction. Paleont., 58, 903-924.

Hunt, D., Tucker, M.E. 1992. Stranded parasequences and the forced regressive wedge systems tract: deposition during base-level fall. Sediment. Geol., 81, 1-9.

Husson, J. M., Higgins, J. A., Maloof, A. C., Schoene, B. 2015a. Ca and Mg isotope constraints on the origin of Earth's deepest $\delta^{13}C$ excursion. Geochim. Cosmochim. Acta, 160, 243-266.

Husson, J. M., Maloof, A. C., Schoene, B., Chen, C. Y., Higgins, J. A. 2015b. Stratigraphic expression of Earth's deepest $\delta^{13}C$ excursion in the Wonoka Formation of South Australia. Amer. Jour. Sci., 315, 1–45.

Imbrie, J. 1985. A theoretical framework for the Pleistocene ice ages. Jour. Geol. Soc., 142,417-432.

Kerans, C., Playton, T., Phelps, R., Scott, S.Z. 2014. Ramp to rimmed shelf transition in the Guadalupian (Permian) of the Guadalupe Mountains, West Texas and New Mexico.

In Vermer, K., Playton, T.E., Harris, P.B. (Ed.) Deposits, Architecture, and Controls of Carbonate Margin, Slope and Basinal Settings. SEPM, 105, 26-49.

Kump, L.R. 1991. Interpreting carbon-isotope excursions: Strangelove oceans. Geology, 19, 299-302.

Li, Y., Montanez, I.P., Liu, Z., Ma, L. 2017. Astronomical constraints on global carbon-cycle perturbation during Oceanic Anoxic Event 2 (OAE2). EPSL, 462, 35-46.

Lu, M., Zhu, M. Zhang, J., Shields-Zhou, G., Li, G., Zhao, F., Zhao, X., Zhao, M. 2013. The DOUNCE event at the top of the Ediacaran Doushantuo Formation, South China: Broad stratigraphic occurrence and non-diagenetic origin. Precamb. Res. 225, 86-109.

Maloof, A.C., Porter, S.M., Moore, J.L., Dudás, F.Ö., Bowring, S.A., Higgins, J.A., Fike, D.A., Eddy, M.P. 2010. The earliest Cambrian record of animals and ocean geochemical change. GSA Bull., 122, 1731-1774.

Morel, F.M.M., Milligan, A.J., Saito, M.A. 2014. Marine Bioinorganic Chemistry. In Holland, H.D., Turekian, K.K. (Eds.). The Role of Trace Metals in the Oceanic. Treatise on Geochemistry, 2nd Edition, 8, 123-150.

Myrow, P.M. and Grotzinger, J,P. 2000. Chemostratigraphic proxy records: Forward modeling the effects of unconformities, variable sediment accumulation rates, and sampling-interval bias. In, Carbonate Sedimentation and Diagenesis in the Evolving Precambrian World, SEPM Society for Sedimentary Geology Special Publication 67, 43-55.

Schiffbauer, J.D., Huntley, J.W., Fike, D.A., Jeffrey, M.J., Gregg, J.M., Shelton, K.L., 2017. Decoupling biogeochemical records, extinction, and environmental change during the Cambrian SPICE event. Sci. Adv., *3*, p.e1602158.

Shannon, C. E., 1949. Communication in the Presence of Noise. Proceed. IRE, 37, 10-21.

Jarvis, I., Gale, A.S., Jenkyns, H.C., Pearce, M.A. 2006. Secular variation in Late Cretaceous carbon isotopes and sea-level change: Evidence from new $\delta^{13}C$ carbonate reference curve for the Cenomanian-Campanian (99.6-70.6Ma). Geol. Mag. 143, 561-608.

Sonnenfeld, M.D. 1993. Anatomy of offlap: Upper San Andres Formation (Permian, Guadalupian), Last Chance Canyon, Guadalupe Mountains, New Mexico in Carlsbad Region (New Mexico and West Texas). In New Mexico Geological Society 44th Annual Fall Field Conference Guidebook. Love, D. W., Hawley, J. W., Kues, B. S., Austin, G. S.. Lucas, S. G. (eds.), 357 pp., 195-203.

Tetzlaff, D. 2023. Stratigraphic forward modeling software package for research and education: *arXiv preprint arXiv:2302.05272*.

Tetzlaff, D., Harbaugh, J.W. 1989. Simulating Clastic Sedimentation. Van Nostrand Reinhold, New York, 202 pp.

von der Heydt, A. S., Ashwin, P. 2016. State dependence of climate sensitivity: attractor constraints and paleoclimate regimes. Dynamics and Statistics of the Climate System, 2016, 1–21.

Wang, Y., Chen, D., Liu, M., Liu, K., Tang, P. 2022. Ediacaran carbon cycling and Shuram excursion recorded in the Tarim Block, northwestern China. Precamb. Res., 377, p.106694.

Wang, Y., Jiang, G., Shi, X. and Xiao, S. 2016. Paired carbonate and organic carbon isotope variations of the Ediacaran Doushantuo Formation from an upper slope section at Siduping, South China. Precamb. Res., 273, 53-66.

Warrlich, G., Bosence, D., Waltham, D., Wood, C., Boylan, A., Badenas, B. 2008. 3D stratigraphic forward modelling for analysis and prediction of carbonate platform stratigraphies in exploration and production. Mar. Pet. Geol., 25, 35-58.

Wood, R.A., Poulton, S.W., Prave, A.R., Hoffmann, K.H., Clarkson, M.O., Guilbaud, R., Lyne, J.W., Tostevin, R., Bowyer, F., Penny, A.M., Curtis, A. 2015. Dynamic redox conditions control late Ediacaran metazoan ecosystems in the Nama Group, Namibia. Precamb. Res., 261, 252-271.

Wu, Q., Ramezani, J., Zhang, H., Yuan, D.X., Erwin, D.H., Henderson, C.M., Lambert, L.L., Zhang, Y.C., Shen, S.Z. 2020. High-precision U-Pb zircon age constraints on the Guadalupian in West Texas, USA. Paleogeog., Paleoclim., Paleoecol., 548, p.109668.

Yuan, L., Zhou, Y., Chen, X., Zhu, M., Poulton, S. W., Tian, Z., Shields, G. A. 2023. Multiple ocean oxygenation events during the Ediacaran Period: Mo isotope evidence from the Nanhua Basin, South China. Precamb. Res., 388, 107004.

Figures and captions

Figure 1: Mixed carbonate-siliciclastic sequence and $\delta^{13}C$ data on a rimmed shelf. A: Schematic, with facies distributions and major surfaces (sequence boundaries/correlative conformities (CC); transgressive surfaces; maximum flooding surfaces; parasequence boundaries) through a full and succeeding partial sequence. The shoreline trajectory traces the timeline of sediment at a fixed water depth through time. B: A Wheeler diagram of (A) showing the actual distribution of facies in space (landward to seaward) and through time. Horizontal lines show non-deposition. Modified from (Sonnenfeld, 1993). VE is vertical exaggeration. C: $\delta^{13}C$ data from a vertical succession through a mixed carbonate-siliciclastic ramp succession at Brak, Ediacaran Nama Group (Omkyk Member), Namibia, showing the distribution of lithologies and the position of parasequence boundaries. Modified from (Wood et al., 2015).

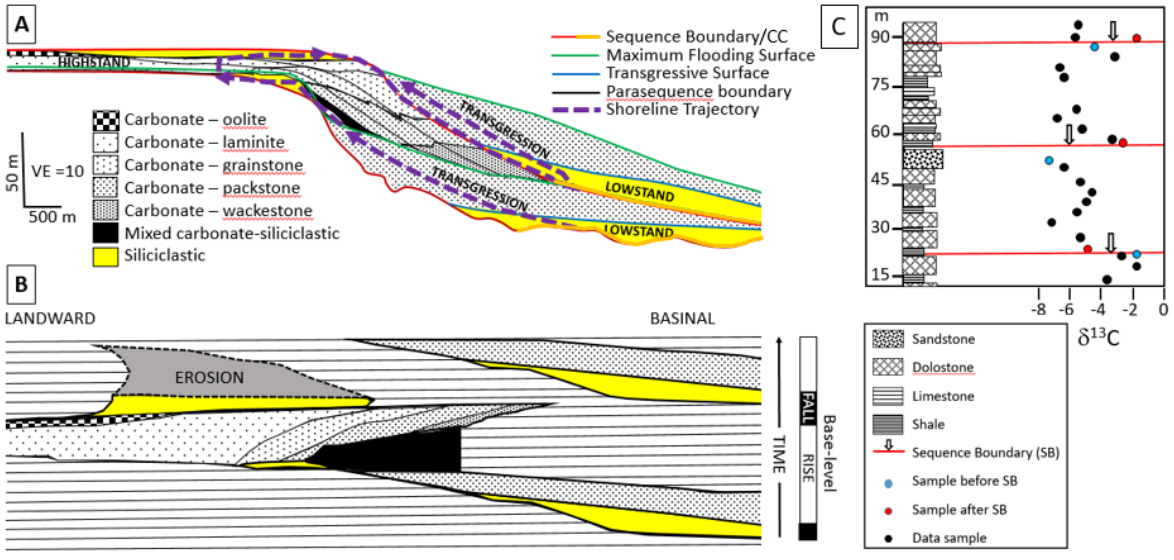

Figure 2: Section through 3D sedimentary succession simulated by geological process model SedSimple over 5 Myr with five 1 Myr relative sea level cycles. A,B,C: Overall rising sea-level (A inset). D,E,F: Overall falling sea-level (D inset). A,D: Distribution of sedimentary facies. B,E: Water depth at time of deposition. C,F: Deposition time within each I Myr cycle.

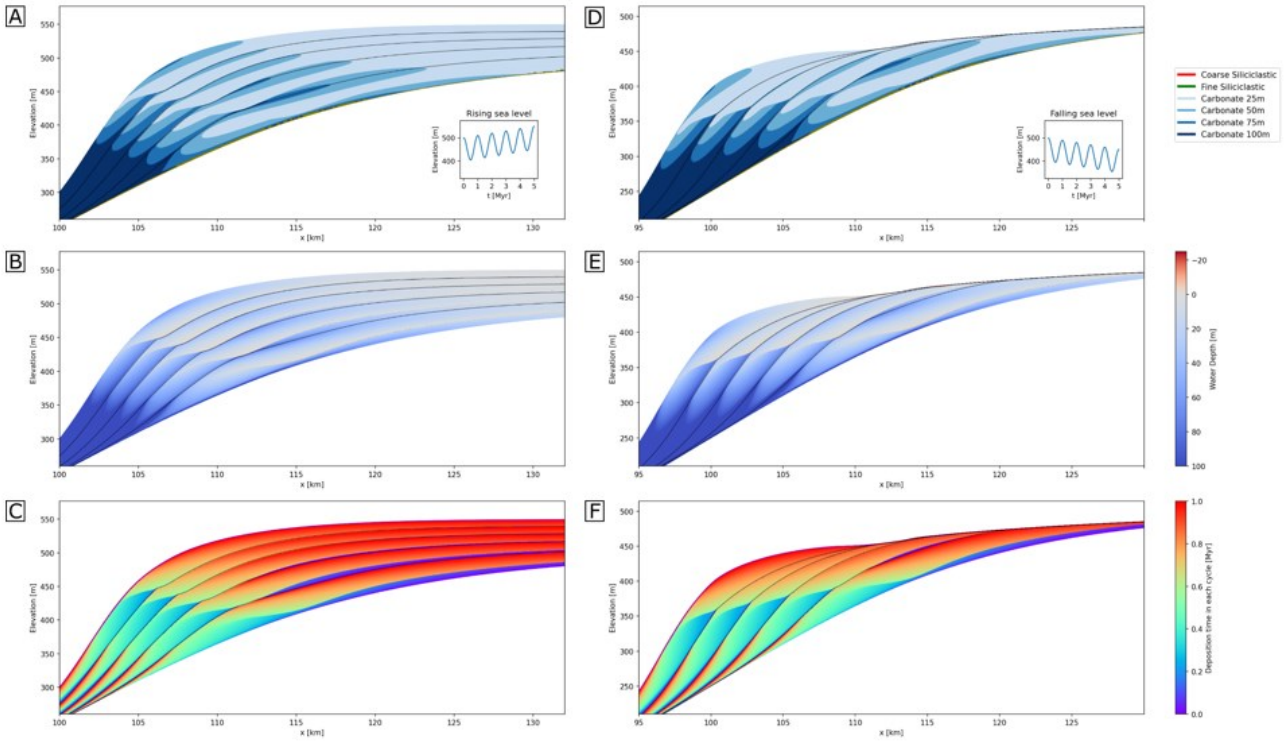

Figure 3: **Cross-sections and vertical transects through 3D sedimentary succession simulated by geological process model SedSimple over 5 Myr with five 1 Myr sea level cycles.** A,C: Overall rising sea-level. B,D: Overall falling sea-level. a) deposition time within each I Myr cycle, with location of six vertical transects. b) distribution of facies deposited through time in each transect. Dotted horizontal sections of curves show hiatuses. c) total percentage of time missing (hiatuses) in each transect. MFS = Maximum Flooding Surfaces. C,D: a) deposition time within two 1 Myr cycles, with location of six vertical transects. b) distribution of facies in each transect through time. Dotted horizontal sections of curves show hiatuses. Regularly spaced geological time samples (red dots between 0.25 and 1 Ma) are projected (arrows) to elevations on each transect at which those times are recorded in the sedimentary record. Dashed arrows show time samples preserved on more than one transect. The distribution of projected points (small triangles in a) is the set of vertical transect sample points that represent regular sampling of geological time.

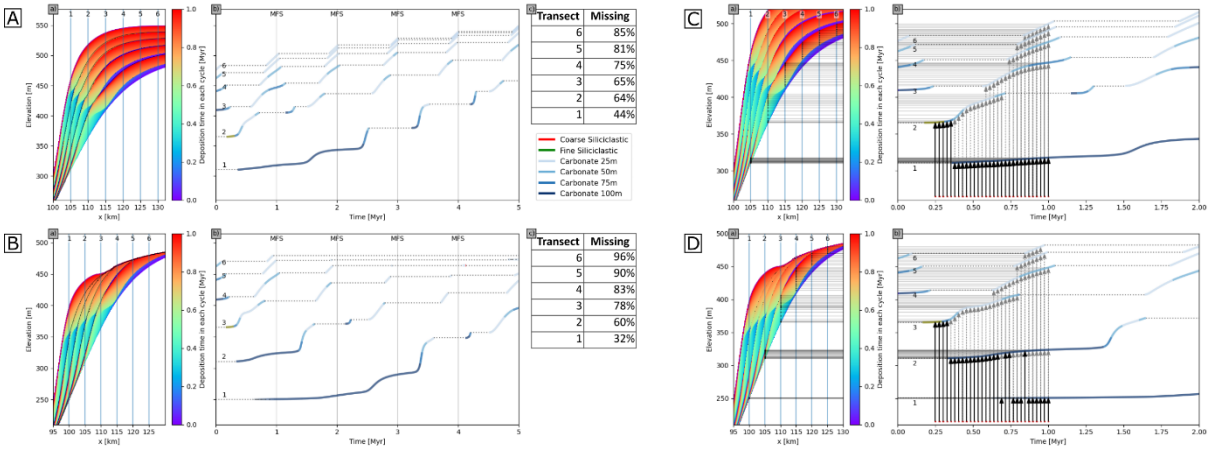

Figure 4: Sections through 3D sedimentary succession showing water depth changes simulated by geological process model SedSimple over 5 Myr with five 1 Myr sea level cycles. A: Overall rising sea-level. B: Overall falling sea-level. a) Water depth of deposition within each 1 Myr cycle, with locations of six vertical transects colour coded. (b) Water depth and $\delta^{13}C$ values in each (colour coded) transect through time, assuming gradient shown on left vertical axis. Grey lines show full water depth history along each transect.

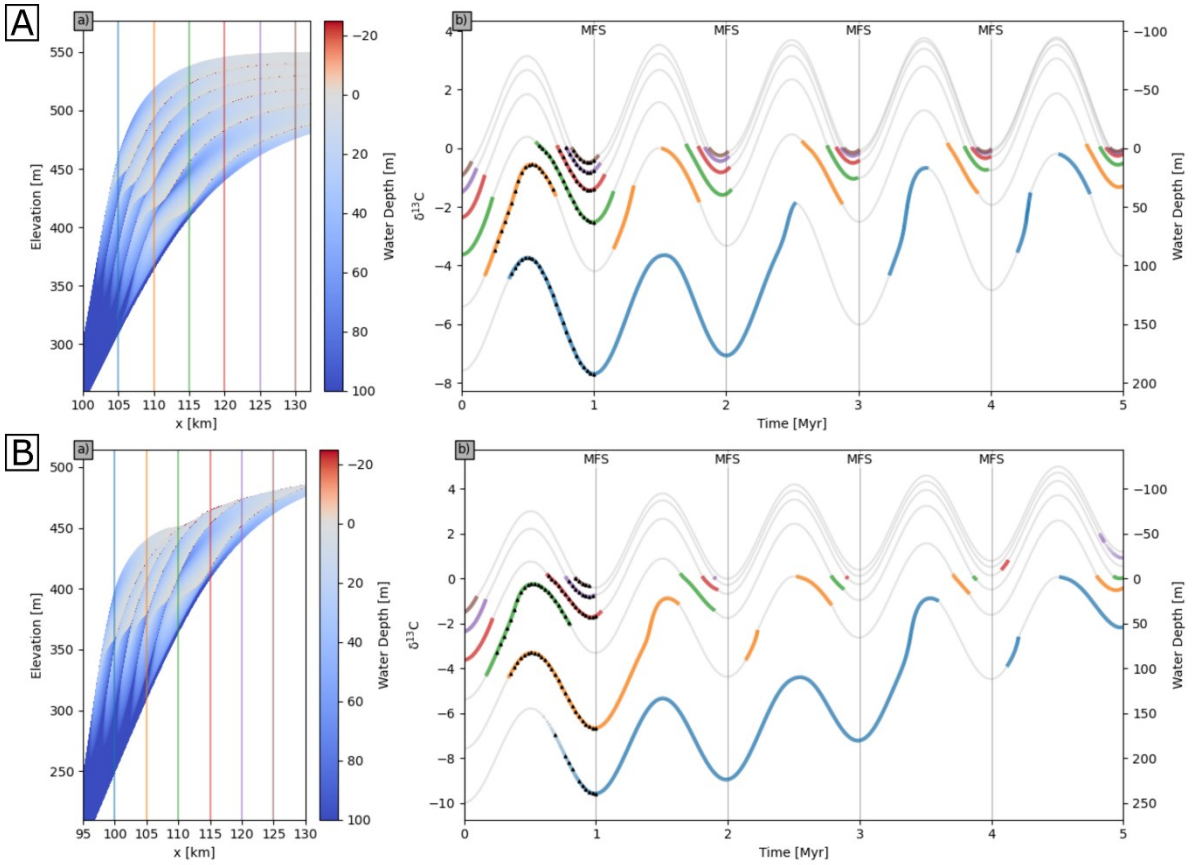

Figure 5: $\delta^{13}C$ values in overall rising sea-level scenario. A: Derived from six transects (a to f; colour coded as in Fig. 4), and all combined (g), plotted by height in a 3D sedimentary succession simulated by geological process model SedSimple over 5 Myr with five 1 Myr cycles, assuming $\delta^{13}C$ gradient shown in Figure 4. B: $\delta^{13}C$ values in A linearly interpolated to time assuming that recorded data span the complete 5 Myr interval, with correct temporal record of preserved sediments shown in black.

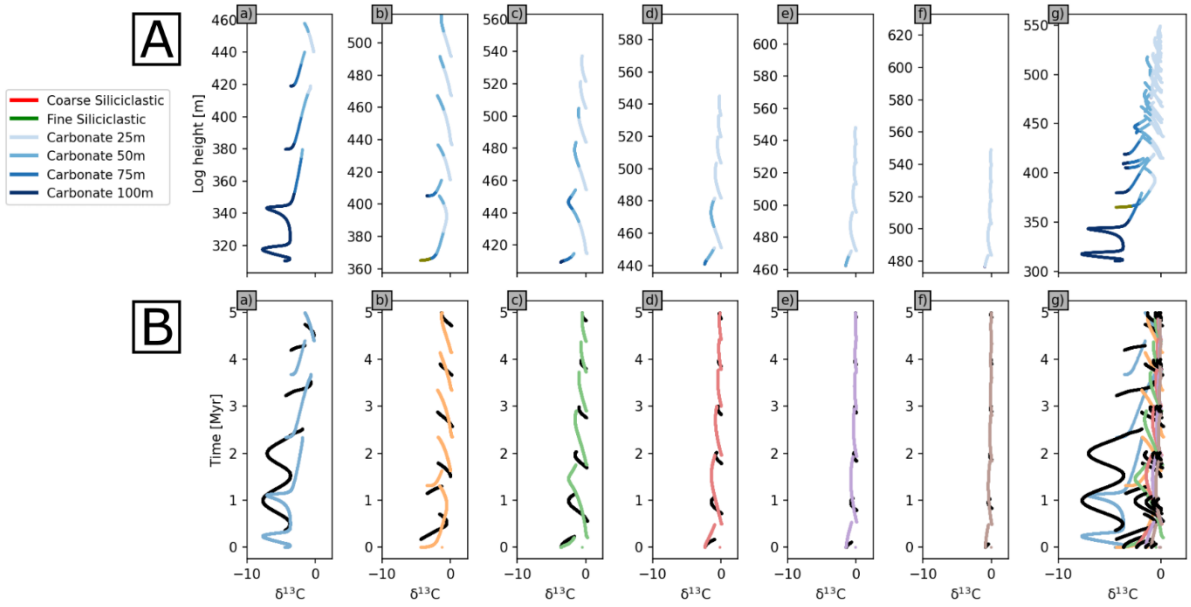

Figure 6: $\delta^{13}C$ values in overall falling sea-level scenario. A: Derived from six transects (a to f; colour coded as in Fig. 4), and all combined (g), plotted by height in a 3D sedimentary succession simulated by geological process model SedSimple over 5 Myr with five 1 Myr cycles, assuming $\delta^{13}C$ gradient shown in Figure 4. B: $\delta^{13}C$ values in A linearly interpolated to time assuming that recorded data span the complete 5 Myr interval, with correct temporal record of preserved sediments shown in black.

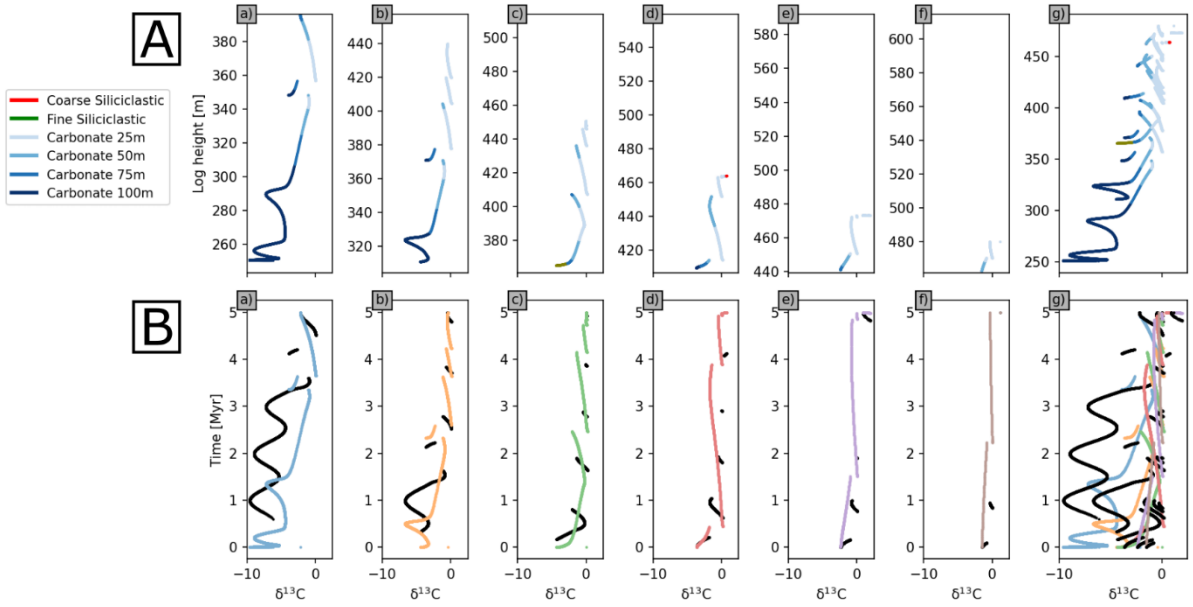

Figure 7: $\delta^{13}C$ values and facies distribution derived from six transects (a to f) plotted by height through a 3D sedimentary succession, simulated by geological process model SedSimple over 5 Myr with five 1 Myr sea level cycles, assuming the $\delta^{13}C$ gradient shown in Figure 4. A,B: overall rising sea-level; C,D: overall falling sea-level. A,C: Interpreted correlation from an experienced stratigrapher; B,D: Correct correlation. Appendix B provides the interpreter's narrative justification for interpreted correlations.

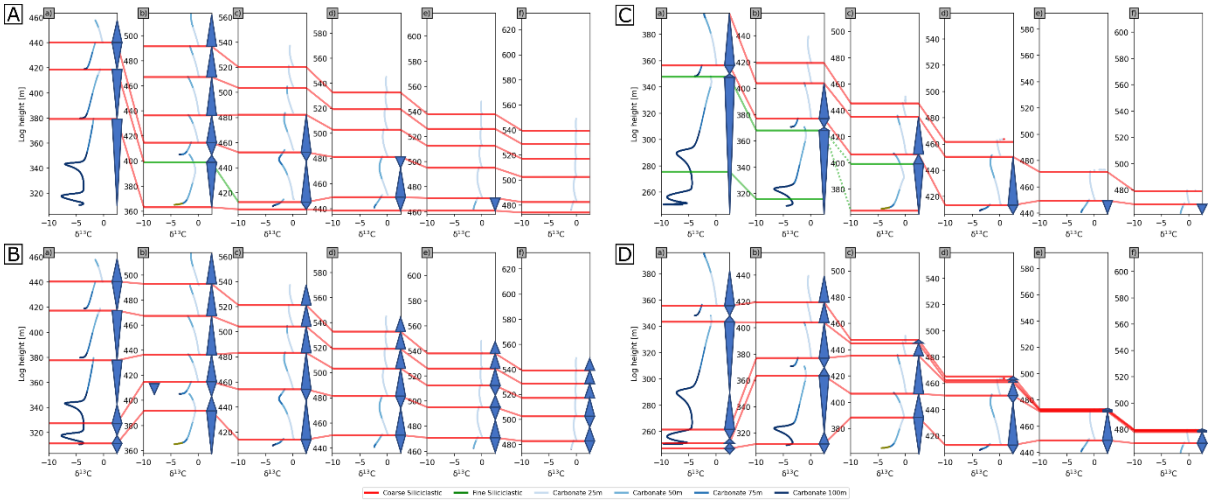

Figure 8: $\delta^{13}C$ values and facies distribution. Derived from six transects (a to f), and all combined (g) by depth through 3D sedimentary succession simulated by geological process model SedSimple over 5 Myr with an overall rising sea-level and five 1 Myr cycles, assuming no $\delta^{13}C$ gradient but three secular changes of $\delta^{13}C$ as shown in insets, by A, depth; B, in time, with correct temporal record of preserved sediments shown in black, and full model spatial output (A) linearly interpolated to time assuming that the recorded data spans the complete 5 Myr interval. Panel F(f) shows apparent cyclicity due to aliasing (dashed red).

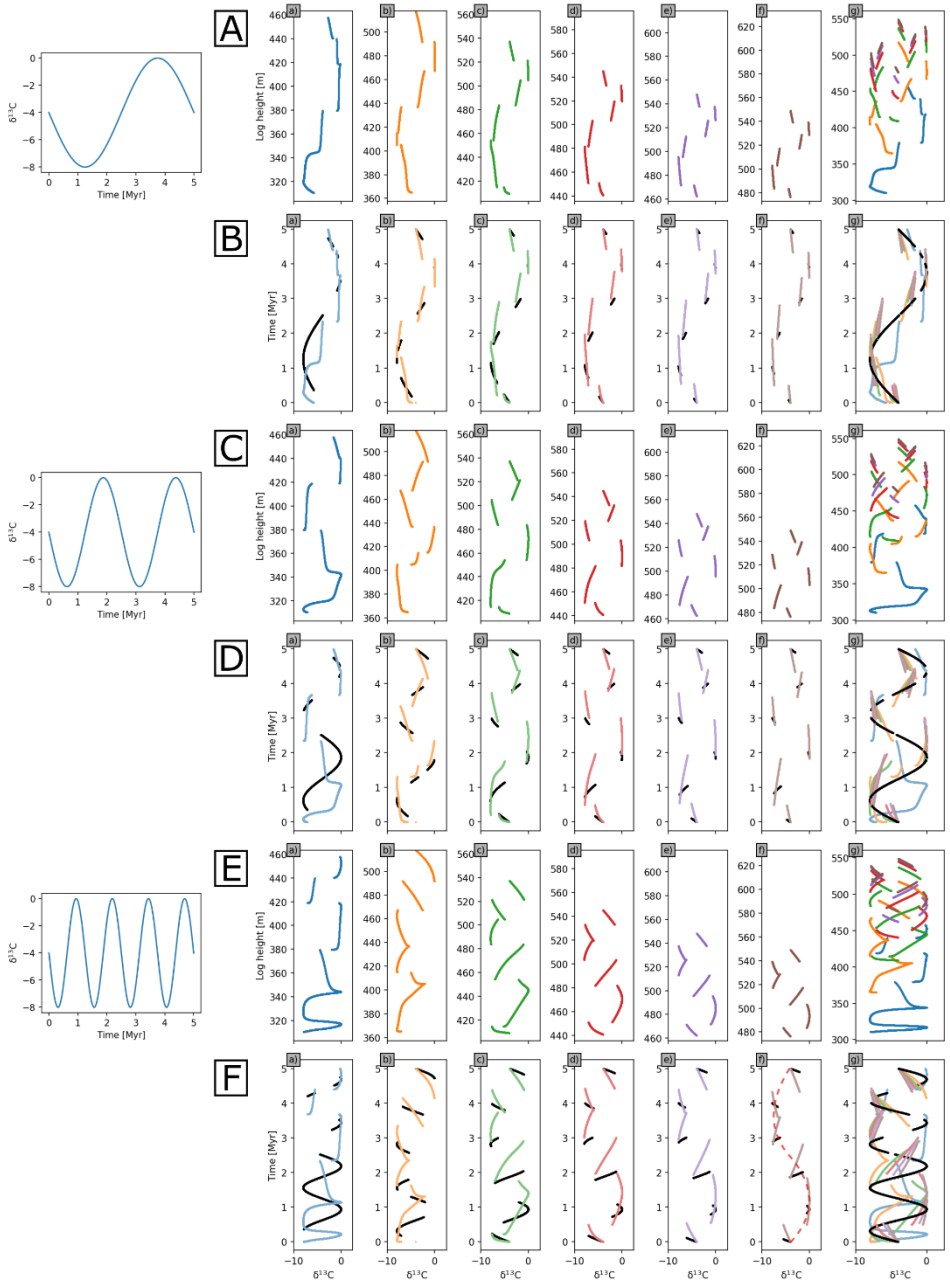

Figure 9: $\delta^{13}C$ values and facies distribution. Derived from six transects (a to f), and all combined (g) by depth through 3D sedimentary succession simulated by geological process model SedSimple over 5 Myr with an overall falling sea-level and five 1 Myr cycles, assuming no $\delta^{13}C$ gradient but three secular changes of $\delta^{13}C$ as shown in insets, by A, depth; B, in time, with correct temporal record of preserved sediments shown in black, and full model spatial output (A) linearly interpolated to time assuming that the recorded data spans the complete 5 Myr interval. Panel F(f) shows apparent cyclicity due to aliasing (dashed red).

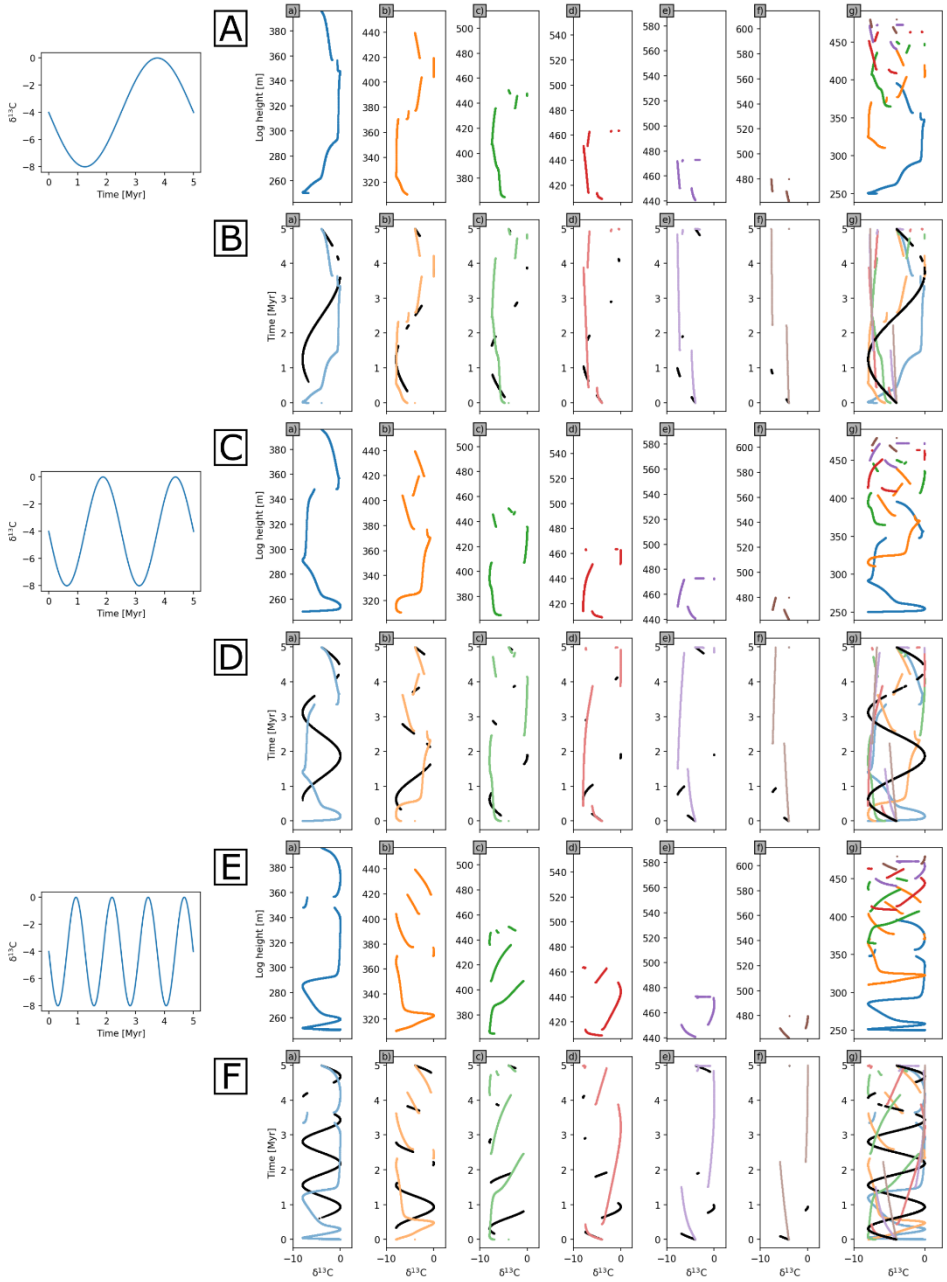

Figure 10: $\delta^{13}C$ values and respective lithologies from a sub-vertically sampled, mixed carbonate-siliciclastic ramp succession at Omkyk, Ediacaran Nama Group (Omkyk Member), Namibia, sampled in every distinct lithological bed at irregularly spaced intervals and showing the position of five high-frequency cycle boundaries. Data points that would have been sampled at approximately regular 0.7 m (A), 1.2 m (B), and 1.6 m (C) intervals are highlighted as large circles and joined by dashed lines.

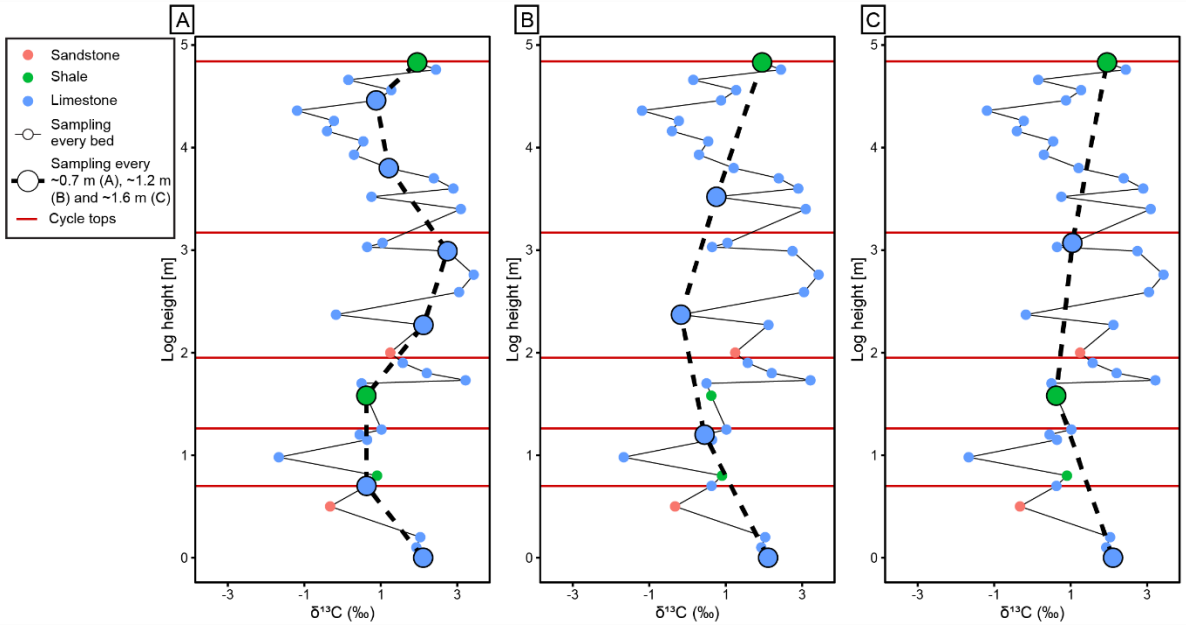

Supplementary Information

Natural sampling and aliasing of shallow-marine environmental signals

Andrew Curtis, Hugo Bloem, Rachel Wood, Fred Bowyer, Graham A. Shields, Ying Zhou, Mariana Yilales, Daniel Tetzlaff

Justification for interpreted correlations

Figure S1

Justification for interpreted correlations

A seasoned and publishing geochemist was asked to correlate cycles in the simulated geochemical transects produced by the GPM. They were given only the logs shown in Figs. 7 and 8 and the following information: the logs were vertical, they are distributed at 5 km spacing from basinward on the left to landward on the right, they were produced by a GPM so that sampling along each profile is effectively infinitely dense, the two scenarios used different sea level variations over time (sea level curves were not provided), and the definition of the six facies. This represents significantly more information than would be available when correlating field samples: the latter always have finite inter-sample spacing, facies are not necessarily precisely defined from field observations, and we do not know which processes or conditions have varied between transects.

The geochemist interpreted the correlations shown in the upper panel of Fig. 10. The geochemist justified the correlations in the following text, as they were produced. The text was returned to the first author in advance of the geochemist having sight of the true

correlations shown in the lower panels. The text below is edited only for grammar, and to refer to our figure numbering.

In both scenarios the following main assumptions were made:

1. There is negligible depth gradient in the carbon isotopic composition of seawater DIC.

2. The sampling resolution is sufficiently high to capture condensed deposition at each MFS (i.e., no δ^{13}Ccarb offset is associated with low resolution sampling in deep sections at each MFS).

Justification for correlations shown in Figs. 7A,B

Observations:

- The oldest strata in section 'a' exhibit two complete negative δ^{13}Ccarb excursions, with falling and rising limbs, which do not appear to show any offset that might otherwise inform temporal hiatuses. The first hiatus is at 380m, consistent with an overall shallowing-up sequence (at least up to 440m).

- The deepest facies in each section appears to correspond with the nadirs of individual d13C excursions. Likewise, the deepest section (a) shows shallowing-up facies during intervals of increasing δ^{13}Ccarb (rising limbs).

Correlation rationale:

- Most negative δ^{13}Ccarb compositions at bottom of section ‘a’ do not correspond with similarly low values in more proximal sections. Assuming an idealised chemostratigraphic approach, this may be used to indicate an older age for strata of section ‘a’ between 380 and 310m than in laterally correlative sections.

- First δ^{13}Ccarb offset in section ‘a’ occurs at 380m, where ‘deepening’ TST sequence appears to be missing above potential sequence boundary. Carbon isotope values in this level may correlate with the lowest values recorded in sections b-f.

- Something interesting is going on in section ‘b’ at ~405m. Possibly conformable sequence boundary indicated by deeper facies overlying shallowest facies, then δ^{13}Ccarb offset at/just below MFS. Slope erosion?

- Sections b-f show δ^{13}Ccarb offsets that might correspond with temporal hiatuses at sequence boundaries, each of which is found at the base of a deepening-up sequence (falling δ^{13}Ccarb limb). The nadirs of each of these falling limbs is progressively muted in shallower sections, which may indicate more extensive truncation of parasequences in more proximal positions, progressive backstepping and transgressive onlap, or a δ^{13}Csw gradient. If either of the latter are correct, then the assumed correlation between sections ‘a’ and ‘b’ is probably incorrect.

Justification for correlations shown in Figs. 7C,D

Observations and correlation:

- Again, the deepest section appears to be more complete. If assuming an idealised chemostratigraphy (negligible δ^{13}Csw gradient), then the stratigraphically lowest interval of

section ‘a’, which exhibits the most negative δ^{13}Ccarb values, might be assumed to be older than any preserved strata in sections b-f.

- Cycles thin considerably in shallower sections, and appear to be progressively lost due to non-deposition or erosion. This is also consistent with deposition of minor coarse clastics at top of section d.

- Sections a and b each exhibit a thin interval where δ^{13}Ccarb is offset to more negative values (~347-357m in section a). In both examples, the offset appears to occur during deepening, above a sequence boundary. This is similar to Case 1, section b (405m). The lower part of this anomaly is quite difficult to correlate further landward than section b.

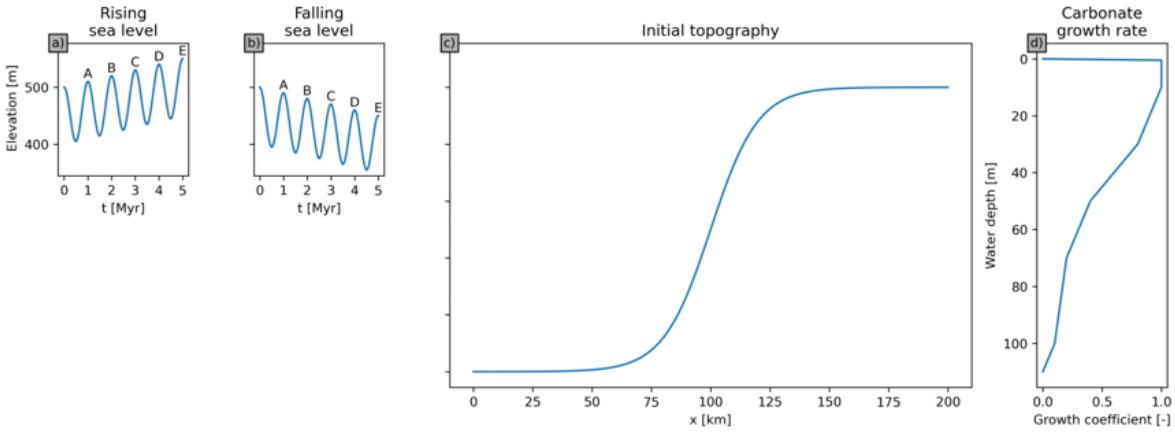

Figure S1. Model parameters used in the geological process model SedSimple over 5 Myr with five 1 Myr cycles. A, overall rising; B, overall falling sea-level; C) initial topography of shelf to basin; D) modelled carbonate growth (production) rate multiplier.